STUDY OF

CERTAIN TETHER SAFETY ISSUES

CONTINUATION OF

INVESTIGATION OF ELECTRODYNAMIC STABILIZATION AND

CONTROL OF LONG ORBITING TETHERS

Contract NAS8-33691

Semiannual Progress Report

For the period 1 September 1981 through 28 February 1982

Volume I

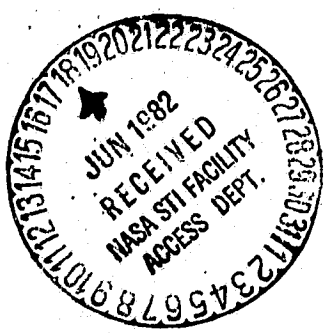

Principal Investigator

Dr. Giuseppe Colombo

Prepared for

National Aeronautics and Space Administration
George C. Marshall Space Flight Center
Marshall Space Flight Center, Alabama 35812

March 1982

Smithsonian Institution
Astrophysical Observatory
Cambridge, Massachusetts 02138

The Smithsonian Astrophysical Observatory
and the Harvard College Observatory
are members of the
Center for Astrophysics

STUDY OF

CERTAIN TETHER SAFETY ISSUES

CONTINUATION OF

INVESTIGATION OF ELECTRODYNAMIC STABILIZATION AND

CONTROL OF LONG ORBITING TETHERS

Contract NAS8-33691

Semiannual Progress Report

For the period 1 September 1981 through 28 February 1982

Volume I

Principal Investigator

Dr. Giuseppe Colombo

Co-Investigators

Dr. Mario D. Grossi
Mr. David Arnold

List of Figures

List of Figures (continued)

List of Figures (continued)

List of Figures (Continued)

List of Tables

TABLE OF CONTENTS

1.0 Introduction

This Semi-Annual Report represents both the work done during this reporting period and the work prior to it in order that all work on "The Study of Certain Tether Safety Issues" be available in a single report. This is Volume I of the Semi-Annual Report required by the contract under which this work was done. Volume II covers work on the study of "Tethers for Payload Orbital Transfer" which ran concurrently.

The "Study of Certain Tether Safety Issues" addresses the behavior of long tethers (10-100 km) in space under two failure situations with potential safety impact: instantaneous jamming of the reel controlling the tether during deployment and cutting of the tether due to a meteor strike or other similar phenomena. Dual and multiple mass point models were used in the SAO SKYHOOK program to determine this behavior. The results of the program runs were verified analytically or by comparison with previously verified results. The study included the effects of tether damping and air drag where appropriate. Most runs were done with the tether system undamped since we believe this best represents the true behavior of the tether. Means for controlling undesirable behavior of the tether, such as viscous dampers in the subsatellite, were also studied.

We assume in the simulations that the system is initially in tension equilibrium. Initial conditions are computed using a small program called DUMBEL which implements the techniques described in Appendix C of the Interim Report for this contract dated March 1981. Wire mass points are spaced as appropriate to the case being studied. In order to simulate a break in the tether, the equilibrium initial conditions are used, but the subsatellite mass and a number of the wire mass points attached to the subsatellite are discarded. Only the motions of the Shuttle and some of the neighboring wire mass points are integrated.

Many special versions of some of the subroutines in the Skyhook software have been developed for various particular studies such as the payload orbital transfer investigation. For this study no special features were required. The basic version of the program is described in the report "The Skyhook Program: A Software Package for a Tethered Satellite System, Including Electrodynamics Interactions," by L.R. Kirschner, May 1980. New versions of modules SKYHOOK, SKYIN2, TENSION,

and TETHER have been used in order to correct some problems in the standard version. These changes are described in a letter from Mr. David Arnold to the principle SKYHOOK users dated 23 October 1980.

This work was carried out under Modification 4 to Contract NAS8-33691 originally titled "Investigation of Electrodynamic Stabilization and Control of Long Orbiting Tethers," Dr. G. Colombo, PI. Concurrent with this effort, SAO also studied under Modification 5 of the same contract "The Use of Tethers for Payload Orbital Transfer" also with Dr. Colombo, PI, and with a subcontract to the Massachusetts Institute of Technology for an engineering study of that concept under the direction of Dr. Manual Martinez-Sanchez, Co-Investigator.

The body of this report has been assembled from the monthy reports submitted under this contract with augmentation where necessary for clarity. This report is intended to stand alone as a summary of the work done of the "Study of Certain Tether Safety Issues." The study results are summarized in Section 2.0.

The authors of this report are Mr. David A. Arnold and Mr. Richard S. Taylor.

2.0 Summary of Results

This section summarizes the results of the tether safety study using the computer plots most representative of the physical behavior of the tether: those showing radial vs. in-plane behavior. These plots give a "side view" of the motion of the tether. Orbital motion of the Shuttle is to the left in these plots whereas time runs to the right (a contradiction which will be corrected in future work). Cases which are representative of the study results are shown here; detailed results are available in the body of the report. All plots show the subsatellite deployed up and assume elastic behavior of the tether.

A reel jam at 10 km during deployment at 20 m/sec is simulated here for the first 800 seconds after the jam. The subsatellite moves ahead of and towards the Shuttle and gets no closer than about 5 km. The same scale is used on both axes. Divide the scale markings by 100 to obtain lengths in meters. No atmospheric drag or damping is used for this plot so the oscillatory motion established by the reel jam will continue indefinitely. The "fold back" at the top of the tether is an artifact of the model and not representative of actual tether behavior. Note the tether mass point nearest the Shuttle which moves ahead of and towards the Shuttle. This behavior is detailed in a later plot and is typical of initial tether behavior in both wire break and reel jam conditions.

This plot duplicates the run shown in the last plot but with ten mass points not six. Note that the same subsatellite motion is obtained but that the "fold back" now occurs at the second mass point indicating that the "fold back" behavior is a result of the discretization in the model. We can conclude that the tether folds back on itself somewhere in its upper third but stays below the subsatellite. Increased discretization also gives further insight into behavior of the tether near the Shuttle where the tether is seen to move ahead of and below the Shuttle.

Here only every fifth configuration from the last run is plotted and another of the general results of this study is clearly shown: initially the tether moves towards the Shuttle as a unit. In those areas where the wire is slack, the actual shape of the tether is undefined and the mass points represent the location of the centers of mass of the slack wire sections which may or may not be on the wire itself. The movement of the tether back towards the orbiter is controllable in this situation by use of a damper in the subsatellite which controls the recoil. This is discussed further below.

Atmospheric drag has been added for this run and a lower recoil velocity used. The general behavior of the tether remains unchanged but it is seen to be considerably less extreme.

A 100 km tether cut at 200 m produces the behavior shown here. Both axes are in centimeters. The 99.8 km length attached to the subsatellite moves away from the Shuttle and does not threaten it. The discretization assumed in these studies leads to the approximation shown here of the true tether behavior. In an actual situation it would be necessary to consider the length of the deployer boom and the attitude of the Orbiter to determine if the tether would drop on to the Orbiter or not. On this scale behavior is very dependent on actual tether characteristics. Other results in the body of this report seem to indicate that the tether may well stream straight forward from the boom and not drop below the boom tip. Further study of actual tether characteristics is necessary before the true behavior can be determined. Once again the tether is seen to move down as a unit initially and then to move ahead of and below the Orbiter, a result which applies to initial behavior in both tether cut and rebound cases. The rebound is fairly slow: the first 50 meter mass point takes fourteen seconds to reach the level of the Orbiter. Behavior of this kind, if indeed it proves to be valid to the inflight situation after further study, can be controlled by tether tapering, tether damping and Orbiter maneuvering or some combination thereof.

As a first step in developing techniques to control rebound behavior we took a look at a subsatellite damper which allows additional tether to be deployed against a spring and viscous damper combination. This system is underdamped. The results of the run are shown graphically on the next two pages.

Note how the damper allows additional tether to be deployed when the reel jams at 10 km. The horizontal scale has been expanded to show the behavior clearly. Actual angular motion of the subsatellite as seen from the Orbiter is less than 1×10^{-3} radian in this example. Further analysis must be done on this subject to optimize damper design.

The underdamped behavior of the system with this damper is clearly seen here where tension at all of the mass points is plotted. Tension in kilograms (approximate) can be read directly from the vertical scale. Peak tension is about 90 kg which is 9 times less than the break strength of 2 mm diameter Kevlar. Note that some sections of the tether still lose tension altogether. Tension ultimately goes to zero in this run (see Section 5.2); other damping characteristics would prevent this but at the expense of longer settling time and greater angular motion as seen from the Orbiter. Clearly this is a promising approach, however, and further study would determine the damping parameters which would fully stabilize the tether in a reel jam situation.

These are the main conclusions of this study which considered upward deployed tethers using 2 mm diameter woven Kevlar rope operating in the elastic range. For the purposes of this study, this material was assumed to have no internal damping, an assumption which we believe will hold true for practical tethers of this material. Other tether material characteristics way prove to be advantageous. For example, "heavy" tethers and tethers with significant internal damping would minimize tether motion during a reel jam or cut. Neither jamming nor cutting during retrieval was studied. This is an area which should be studied to determine those operating conditions which would prevent the subsatellite from hitting the Shuttle in such a failure during all phases of retrieval and/or identify Shuttle maneuvers to achieve the same end.

The results of this study are the basis for further work to define the control laws, Orbiter maneuvers and TSS characteristics necessary to assure safe operation of the system.

The goal of follow-on analyses should be a full understanding of tether system dynamics under normal and failure mode conditions which would lead to identification of operating methods and parameters to optimize useful subsatellite operating time while assuring TSS facility, Orbiter and crew safety.

The SAO SKYHOOK program and its software relatives and derivatives provides the means for SAO to support this goal in a close working relationship with MSFC, JSC, the TSS facility subcontractor and the subsatellite developer.

3.0 Tether Behavior--Wire Break Case

3.1 Tether Modelled As One Mass Point

In order to study the dynamics of the wire after a break, the following test case has been set up. A Shuttle weighing 100 metric tons is in a circular orbit at 220 km altitude with a 300 kg subsatellite deployed upward on a 10 km tether, 2 mm in diameter with a density of 2.5 and elasticity 7×10^{11} dynes/cm^2. The wire is represented by nine 7.853 kg masses spaced at 1 km intervals between the Shuttle and the subsatellite. The tension at the top is 1.24×10^6 dynes. The wire stiffness is 2.199×10^4 dynes/cm for the whole wire and 2.199×10^5 dynes/cm for each wire segment. The bottom segment is stretched 6.315 cm in equilibrium.

In the first run, the motion of the Shuttle and the wire mass adjacent to it are integrated for 200 seconds. The wire mass acquired a radial velocity toward the Shuttle of 33.4 cm/sec. The maximum radial displacement of 13.4 meters occurred in about 80 seconds. The mass returned to its original position at 160 seconds and rebounded. The in-plane displacement was 3.36 meters forward at 160 seconds.

In the SKYHOOK program, each wire mass having the lumped properties of a segment of the wire is connected to the masses on either side by a massless spring with a damping coefficient specified as input data. In this run, the damping coefficient was set to a negligible value since the wire will probably have very little hysteresis. In the case of a single wire mass it is possible to develop fairly accurate analytical formulas for predicting the behavior of the system.

With the wire modelled as a single lump, the radial velocity v_r acquired during recoil is given by $v_r^2 = T^2/mk$ where T is the wire tension m is the wire mass, and k is the stiffness of the section of wire. Substituting the values of T, m, and k, we have v_r = 33.4 cm/sec. which agrees with the observed velocity in the numerical integration. The formula for v_r can be further developed by substituting the expressions $m = \rho A\, dl$, and $k = EA/dl$ where A is the cross sectional area of the wire, ρ is the density, dl is the length of the segment, and E is the elasticity. This gives:

$$v_r^2 = T^2/\rho E A^2$$

or,

$$v_r = T/A\sqrt{\rho E} \quad .$$

It is interesting to note that the recoil velocity v_r is independent of the length dl of the wire segment.

In this simple model with only one wire mass point, the wire mass goes into a free orbit once the wire contracts to the point where the tension goes to zero. Given the position and velocity of the wire mass at the point the tension goes to zero the orbital elements of the mass can be computed as follows. The semimajor axis a of the orbit is

$$a = 1/(2/r - v^2/GM)$$

where r is the distance from the center of the earth, v is the magnitude of the total velocity and GM is the gravitational constant times the mass of the earth. We have used 3.986013×10^{26} for the value of GM in cgs units. Defining h as L/m where L is the orbital angular momentum, the eccentricity e of the orbit is

$$e = \sqrt{1 - h^2/GMa} \quad .$$

The perigee P of the orbit is $a(1 - e)$. The distance dr that the mass recoils toward the Shuttle is $dr = r - P$ where r is the initial geocentric distance. If dr is small compared to the length of the segment of wire, the behavior of the wire after a break should be relatively stable. The time required for the mass to make its closest approach to the Shuttle can be calculated from the equation for an ellipse, namely

$$r = a(1 - e^2)/(1 + e\cos(\theta - \theta_0))$$

where θ_0 is the angle at perigee. The angle from the initial point to perigee can be obtained from the equation

$$\cos(\theta - \theta_0) = (a(1 - e^2) - r)/ er$$

where r is the initial distance from the center of the earth. The time t required to reach perigee is approximately $(\theta - \theta_0)/\omega$ where ω is the orbital angular velocity.

The time during which the wire is accelerated toward the Shuttle can be easily computed since it is just 1/4 of a cycle of a simple harmonic oscillator. In the simple one-lump model, the frequency of the longitudinal oscillation is $f = \sqrt{k/m}$. The period is $2\pi/f$ and a quarter cycle is therefore $\pi/2f$. Substituting the values of k and m we have .2968 sec for the

acceleration phase of the recoil. In the numerical integration the acceleration time was .297 sec, in good agreement with the calculated value.

The tension T in the wire can be computed approximately, neglecting the mass of the wire using the formula

$$T = 3GMm_\rho l'/r_o^2$$

where r_o is the radius of the orbit of the center of mass of the Shuttle plus end mass, and l' is the distance from the center of mass to the end mass m_ρ. This formula can be used more conveniently in parametric studies of cases where the mass of the wire is not too large compared to the payload.

A small program was written to compute the amount of recoil and the time to closest approach using the formulas developed above. Runs have been done using various values of the length dl of the section of wire remaining after the break. Total wire lengths of 10 and 100 km have been studied. The table below lists the results. The first column is the total wire length l, the second column is the length of wire dl attached to the Shuttle after the break, the third column is the amount of recoil dr, the fourth column is the closest approach to the altitude of the Shuttle, namely dl - dr. All distances are given in kilometers. The fifth column is the time to closest approach in seconds.

Table 1

Recoil Distance and Time of Closest Approach for Various Distances to the Break

l	dl	dr	(dl-dr)	t
10	2.	.0055	1.9945	36.5
10	1.	.011	.989	74.
10	.5	.022	.477	151.
10	.2	.050	.140	392.
10	.1	.120	-.020	747.
100	10.	.111	9.889	74.
100	5.	.228	4.772	151.
100	2.	.599	1.401	392.
100	1.	1.197	-.197	747.

In the case of the 10 km wire the velocity computed at the end of the acceleration phase using the analytical formula is 30 cm/sec and for the 100 km wire it is 3 meters/second. These velocities are a little smaller than in the numerical integration because they were computed with a smaller tension force that neglects the mass of the tether itself.

Examining the results shown in the table leads to two conclusions. First, the amount of recoil dr seems to be approximately inversely proportional to the length dl of the remaining piece of tether. Second, the values of dl and dr seem to scale with the total length l. The time required to reach closest approach depends on the ratio of dl to l.

The results described so far treat the wire as a single lump. In the next case considered the wire is represented by two lumps at distances of 1 and 2 km from the Shuttle. The velocity acquired by the end wire mass (No. 2) was 34 cm/sec, and the velocity of the center wire mass (No. 3) was 20 cm/sec. The value predicted analytically, treating the wire as a single lump is 30 cm/sec, as mentioned previously. The values of recoil dr for masses 2 and 3 were 9.1 and 8.6 meters. The in-plane displacements were .9 and .85 meters, and the times t of closest approach were 51 and 57 sec respectively. These values are intermediate between the results given in the table above for dl equal to 1 and 2 kilometers.

The gradient of the gravitational and centripital accelerations tends to stretch the tether. In the case above, masses 2 and 3 are initially moving closer together. However, the gradient forces counteract this movement and after 30 sec the masses come into tension and rebound. The maximum amplitude of the oscillation is about .5 meters. It is because of this coupling between the masses that the behavior is intermediate between the 1 and 2 km cases calculated analytically.

The fact that the recoil velocity in the single lump model is independent of the length of the wire segment, together with the results of the two lump run above seem to suggest that the wire recoils such that all parts end up moving at the same velocity.

The runs do not include the effects of atmospheric drag. In the case of upward deployment, the coriolis forces are in the forward direction when the wire recoils downward. Drag is of course to the rear. In order

to see which effect dominates in a sample case, the run with two wire masses (representing 2 km of wire) described above has been rerun including drag. The in-plane displacement was about .9 meters forward after 60 seconds without drag. With drag, the displacement after 60 seconds was about 2.8 meters to the rear, indicating that drag dominates by a few factors in this case.

3.2 Tether Modelled as Five Mass Points

A run has been prepared with five mass points representing the wire to study the behavior of the various parts of the section attached to the Shuttle after a break. All the parameters are the same as in Section 3.1 except that the piece attached to the Shuttle is now five kilometers long. A computation using the analytic expression given in Section 3.1 gives a recoil of 2.17 meters and closest approach in 14.5 seconds for a five km piece of wire treated as a lump at five km from the Shuttle. In the integration, output data was recorded at one second intervals. The integration was slow with many discontinuities caused by sections of wire going in and out of tension. The run was terminated after 18 seconds of orbital time. Figure 1 shows the radial vs. in-plane behavior of the wire. The in-plane movement resulting from Coriolis forces is greatly exaggerated in this plot. The radial motion does not show on this plot scale.

In order to study the radial behavior, a tabulation of the radial component for each mass has been used. The first item of interest is the velocity distribution along the wire. By differencing successive values, the table of velocities below as computed at 1 second and at 17 seconds.

Table 2

Radial Velocity of Each Mass Point in a Tether Cut at Five Kilometers

Mass	1. sec	17. sec
2	33.81 cm/sec	9.275 cm/sec
3	33.72	9.760
4	34.05	10.024
5	33.64	10.33
6	23.64	18.17

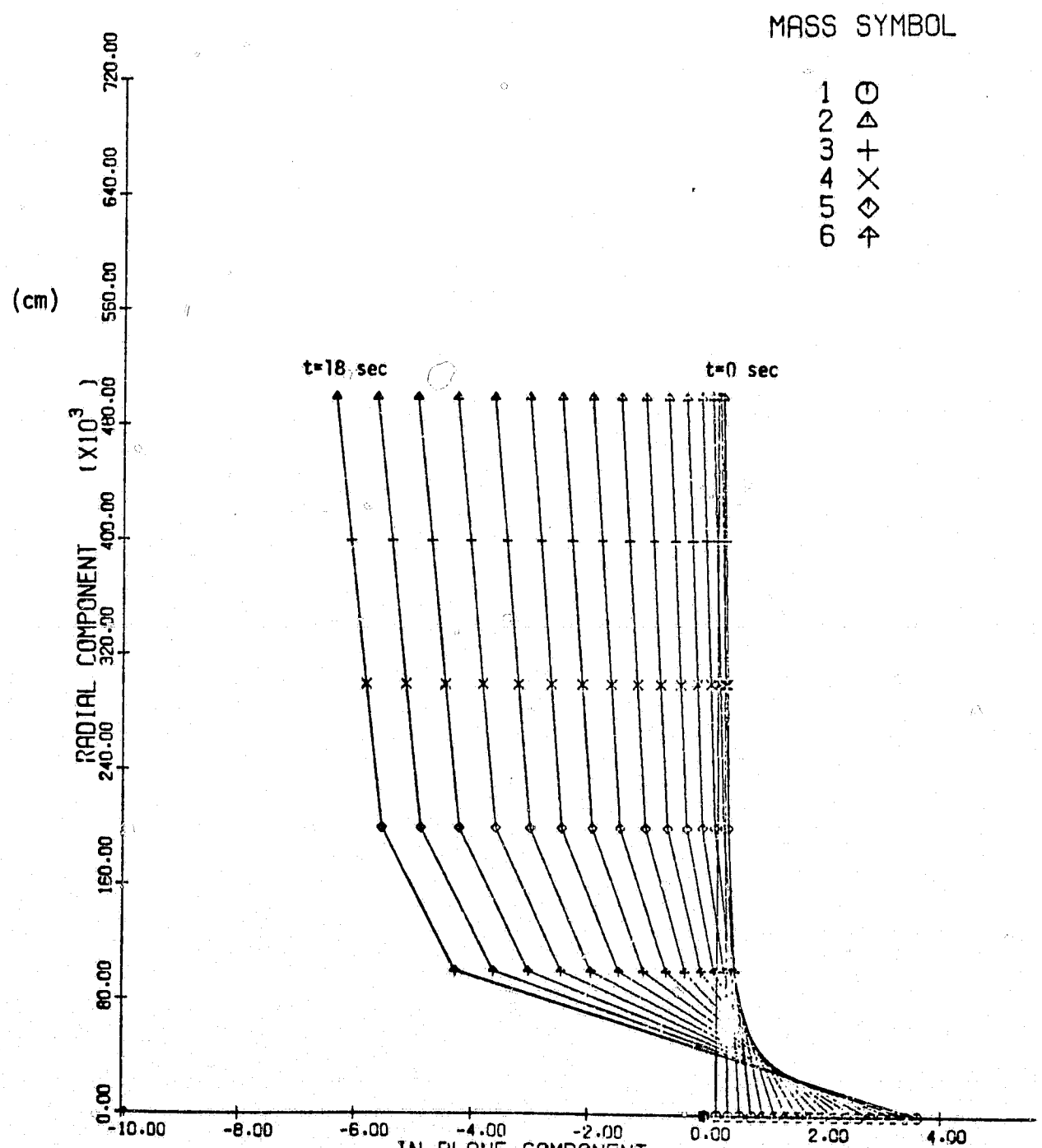

Figure 1. Radial vs. in-plane behavior for the first eighteen seconds after a 10 km tether is cut at 5 km.

The main feature seen from the table is that the whole wire acquires nearly the same velocity. Point number 2 is at the top end of the wire and point number 6 is next to the Shuttle which is mass number 1 by convention. The behavior of the sixth point is anomalous in that it acquires a lower velocity initially but maintains that velocity longer. After the point at the broken end of the wire starts to recoil, the mass next in line starts to recoil also and the result is a longer acceleration time for the end mass. This behavior is repeated down the line except for the mass next to the Shuttle. The Shuttle recoils toward the wire slightly, reducing the acceleration of the sixth mass.

The spacing between each of the masses as a function of time has been computed and tabulated. The spacing between masses 2 through 5 oscillates in the vicinity of .99993 kilometers after the initial contraction of about 7 centimeters. This is approximately the natural length of the wire under no tension. The spacing between 5 and 6 decreases to .99955 km at about 9 seconds, and then increases again almost arriving back to the natural length of the segment by the end of the run. The spacing between 6 and 1 (the Shuttle) decreases to .99630 km at 18 seconds in a monotonic fashion and has not reversed direction by the end of the run.

The run described above confirms in more detail the tentative conclusion reached in the last section. Namely, the wire recoils more or less as a unit after a break. The gradient forces provide a stretching tendency with the sections of wire oscillating near their natural length. The wire orbits more or less as a unit in an orbit approximately the same as a particle at the center of mass.

Since the longitudinal oscillations of the masses representing the wire have rather short periods (on the order of one second), the run was repeated for the first 5 seconds with output points every tenth of a second in order to see the longitudinal oscillations. Figure 2 shows a plot of the tension as a function of time for all segments. It takes approximately one second for the loss of tension to propagate along the five kilometer wire. The theoretical value for the velocity v of propagation of stress along the wire is $v = \sqrt{E/\rho} = 5.29$ km/sec, where E is the elasticity and ρ is the density. After the first second, various segments come in and out of tension for the remainder of the run.

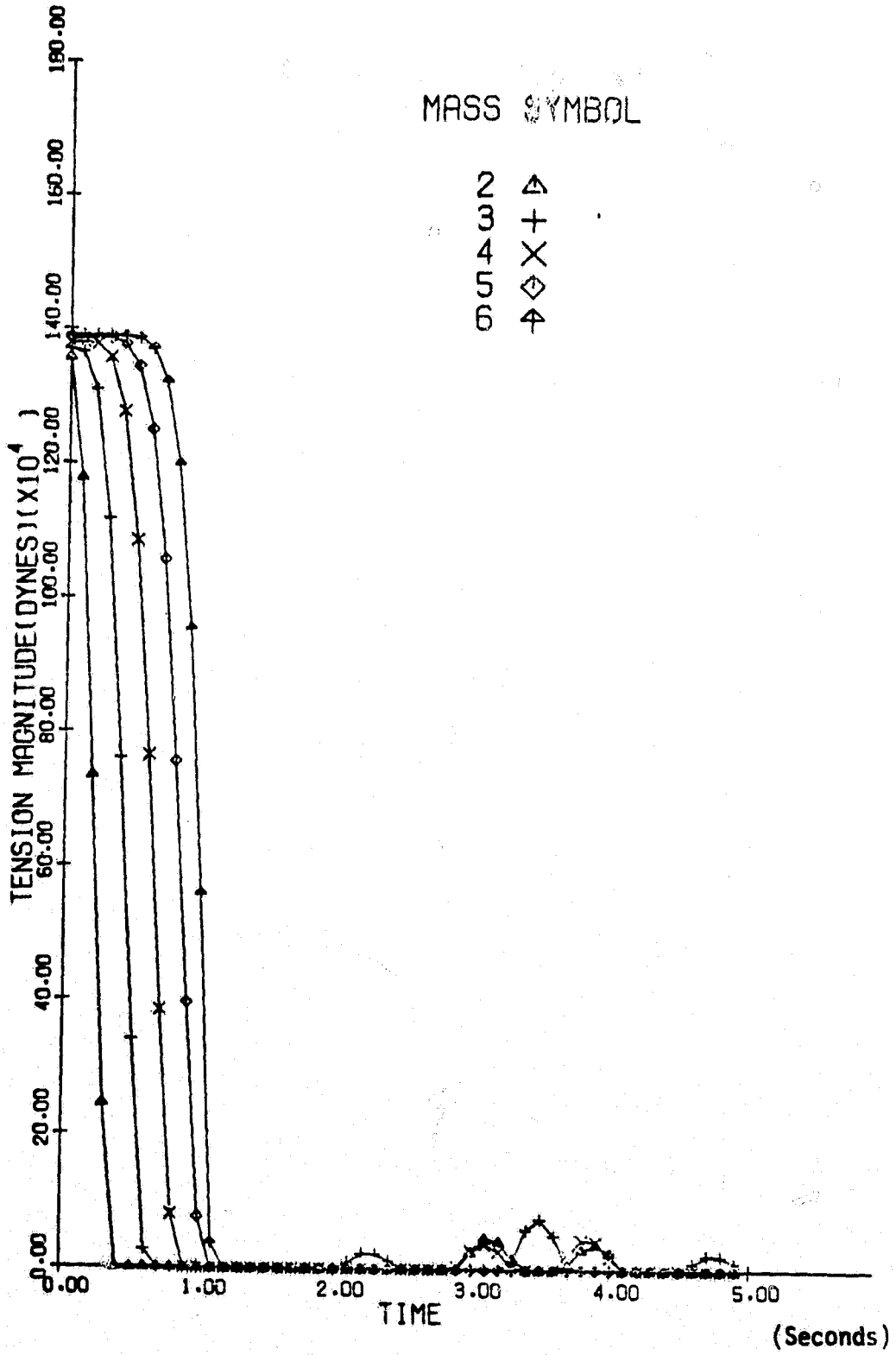

Figure 2. Tension vs. time for a 10 km tether cut at 5 km.

One of the main items of interest from the point of view of studying the recoil of the wire is the behavior of the radial component vs. time. Unfortunately, the motion does not show up on plots such as Figure 1. Plotting the radial component to show features such as the relative motion of the various parts of the wire is complicated by four factors: 1) the radial displacements required to cause loss of tension are small compared to the length of wire; 2) the downward displacement of the wire is large compared to the relative movement of the masses with respect to each other; 3) the initial contraction of the wire is large compared to the subsequent relative displacements of the masses; and 4) the behavior of the point next to the Shuttle is anomalous and shows large displacements relative to the rest of the wire masses.

A small computer program has been written to process the file of radial components in order to make the features of interest show up on a plot of the radial component. Problem 1) can be handled as follows. Subtracting the first value of the radial component for each mass eliminates the large numbers associated with the length of the wire and shows the motion relative to the initial value. In order to separate the plots for each mass a constant can be added to the values for each mass with the spacing arranged so that the plots do not overlap. Figure 3 shows the radial component vs. time with a spacing of 100 cm between each mass. Figure 4 shows the radial vs. in-plane behavior. The time at which each mass begins to recoil can be clearly seen in Figure 3. The dominant feature in Figure 3 is the downward movement of the wire as a whole.

Problem 2) involving the movement of the wire as a whole has been addressed by using one of the masses as the origin and plotting the position of the other masses relative to it. Figure 5 shows the result a) with the mass next to the Shuttle as origin, and b) with the top mass as origin. The two features evident in Figure 5 are the initial contraction of the wire and the anomalous behavior of mass 6 which is closest to the Shuttle. Masses 2 to 5 are gaining on the sixth mass as they all recoil. The spacing between the plots is 35 cm.

Problem 3) can be handled by eliminating the first part of the plot up to about 1 second. Problem 4) can be handled by ignoring the mass next to the Shuttle. This has been done by adding a facility in the processing program for keeping the radial component for one of the masses fixed at a

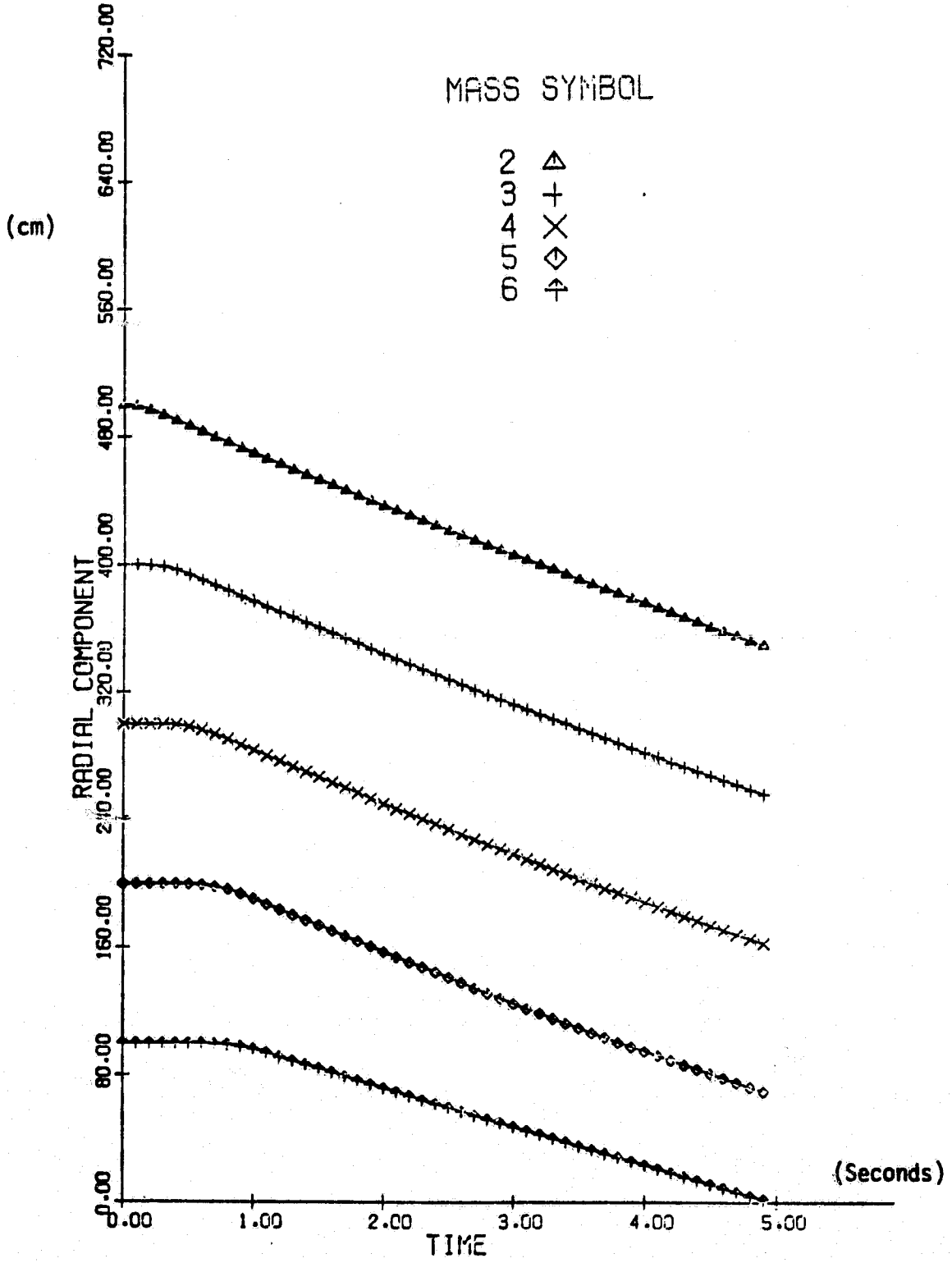

Figure 3. Radial motion vs. time for a 10 km tether cut at 5-km expanded scale.

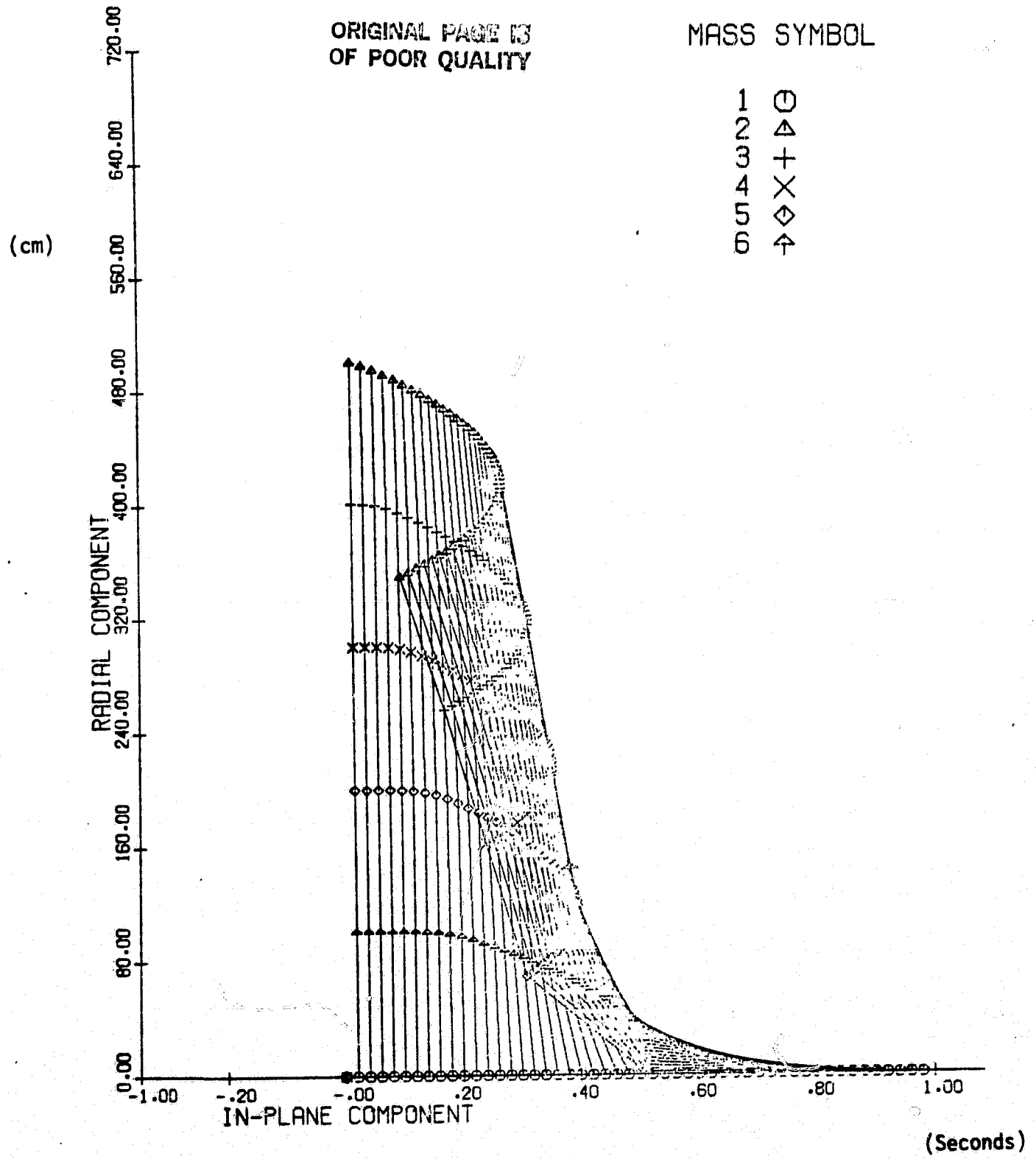

Figure 4. Radial vs. in-plane behavior for a 10 km tether cut at 5 km - expanded scales.

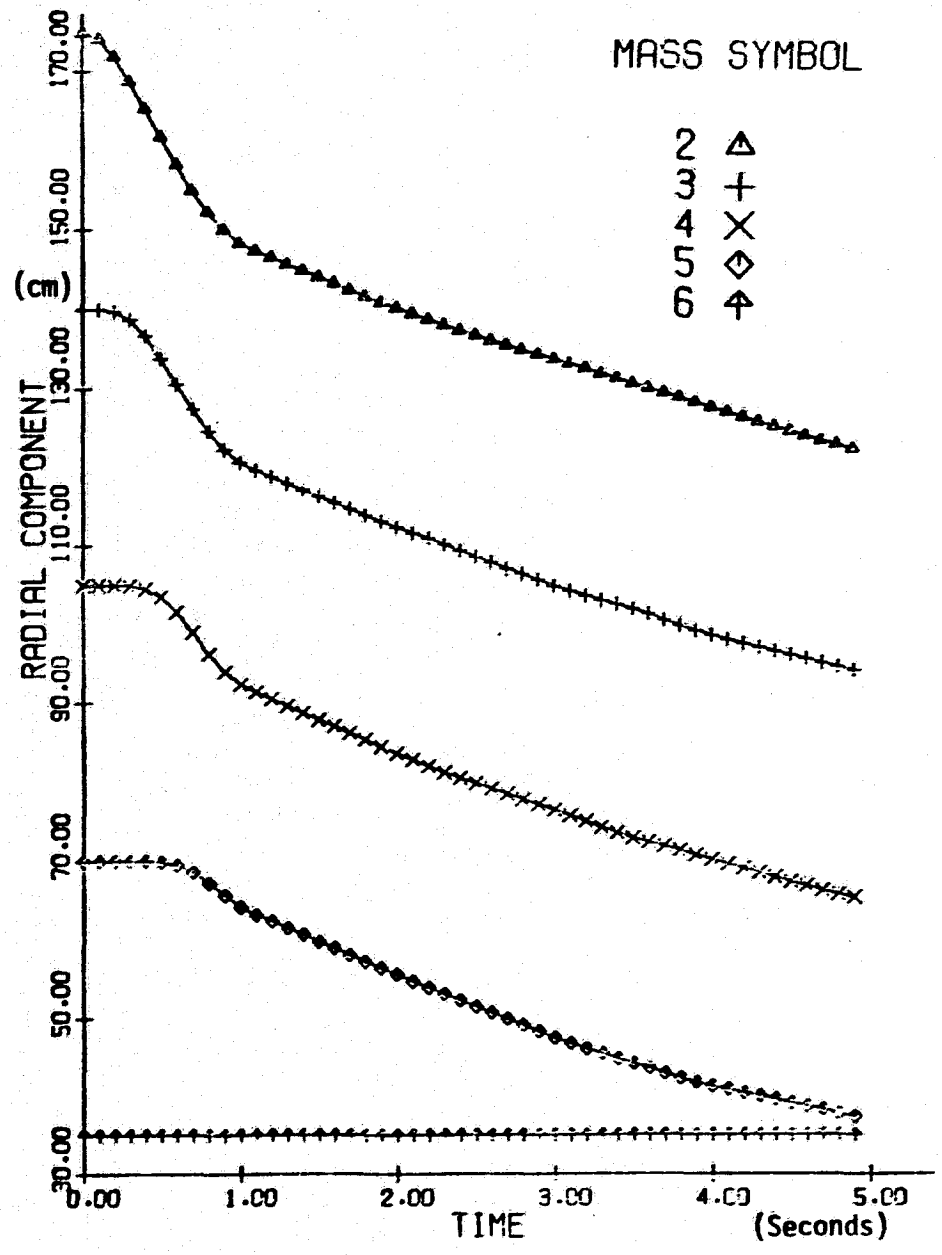

Figure 5a. Relative radial motion vs. time for a 10 km tether cut at 5 km - expanded scale, mass next to shuttle as origin.

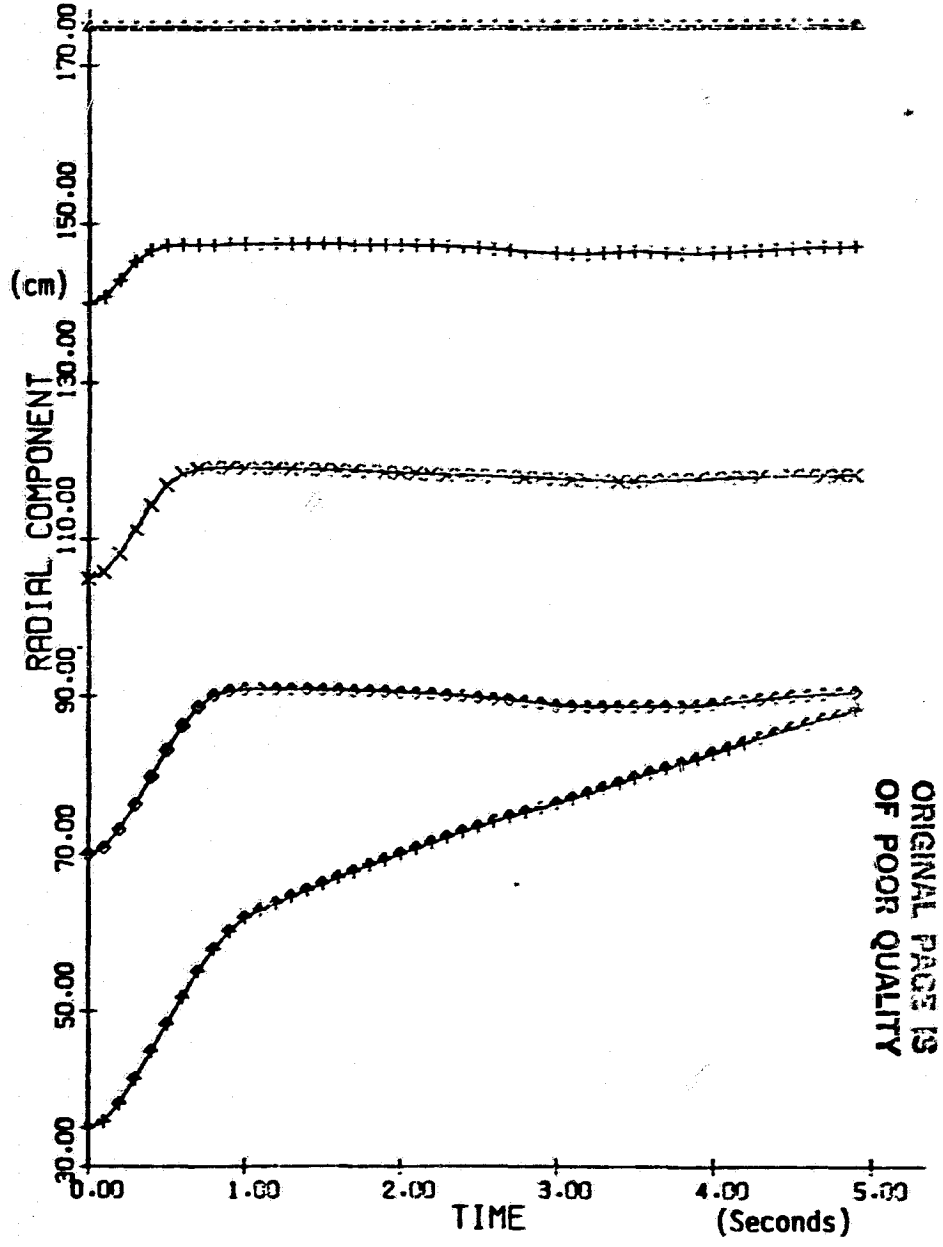

Figure 5b. Relative radial motion vs. time for a 10 km tether cut at 5 km - expanded scale, top mass as origin.

constant value. In Figure 6, the points previous to 3.8 seconds have been deleted, the top mass (number 2) has been taken as the origin, the bottom mass (number 6) has been held fixed, and the spacing between plots is set to 2 cm. The relative motions between masses 2 to 5 show up clearly on this plot. The end of the contraction between masses 4 and 5 is evident as the sharp slope of the beginning of curve 5. Figure 7 shows the tension for each mass beginning at 1.1 seconds when the tension for mass 6 has reached a suitably low value as seen from Figure 2. The convention used here is that the tension plotted is the tension between the numbered mass and the next higher numbered mass. In the case of mass 6 it is the tension between mass 6 and the Shuttle which is mass 1 by convention. There are two tension spikes between masses 2 and 3 at about 3.1 and 3.9 seconds. These correspond to the two minima of curve 3 in Figure 5. There are three tension spikes between 3 and 4, and two between 4 and 5. Mass 6 does not reestablish tension with either 5 or 1 in this plot.

3.3 Effect of Level of Discretization of Model on Tether Behavior

3.3.1 No Damping

In runs done previously for a broken tether it was noted that the velocity acquired by the wire mass closest to the Shuttle is significantly lower than the velocity of the other masses. This effect is presumably a result of the discrete representation of the wire. If a smaller spacing were used we would expect that only the last point, which now represents a smaller section of wire, would show the effect. A series of runs has been done with a 5 km wire divided into 5, 10, and 20 sections to see the effect of discretization in the modelling of a break 5 km from the Shuttle. In order to compare results with runs done on the Skyhook program, similar parameters have been used in the one-dimensional program. The values used are wire diameter .2 cm, length 5 km, Shuttle mass 100 metric tons, wire tension 1.35×10^6 dynes, wire density 2.5, and elasticity $.7 \times 10^{12}$ dynes/cm^2. Figure 8 shows the velocity profile 2.0 seconds after the break. Parts a, b, and c, are with 5, 10, and 20 sections respectively. The first column is the velocity in cm/second. The velocities of the wire masses obtained with the Skyhook program for the 5 wire masses are 33.8, 33.7, 34.0, 33.6, and 23.6 cm/sec as reported in Table 2. Comparing the three parts of Figure 8 it appears that the last couple of points on either end

Figure 6. Relative radial motion vs. time for a 10 km tether cut at 5 km - expanded scale, top mass as origin, bottom mass (#6) held fixed.

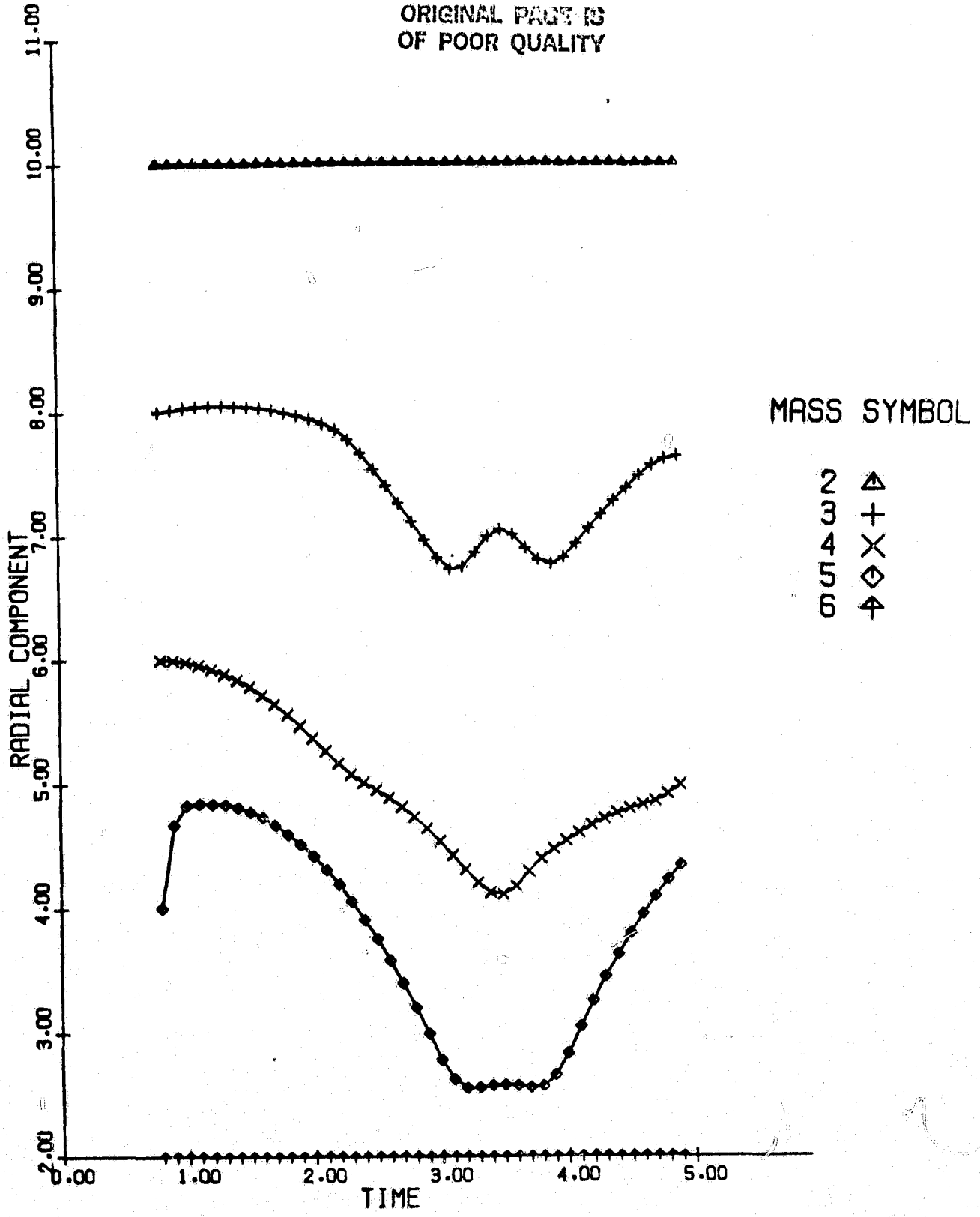

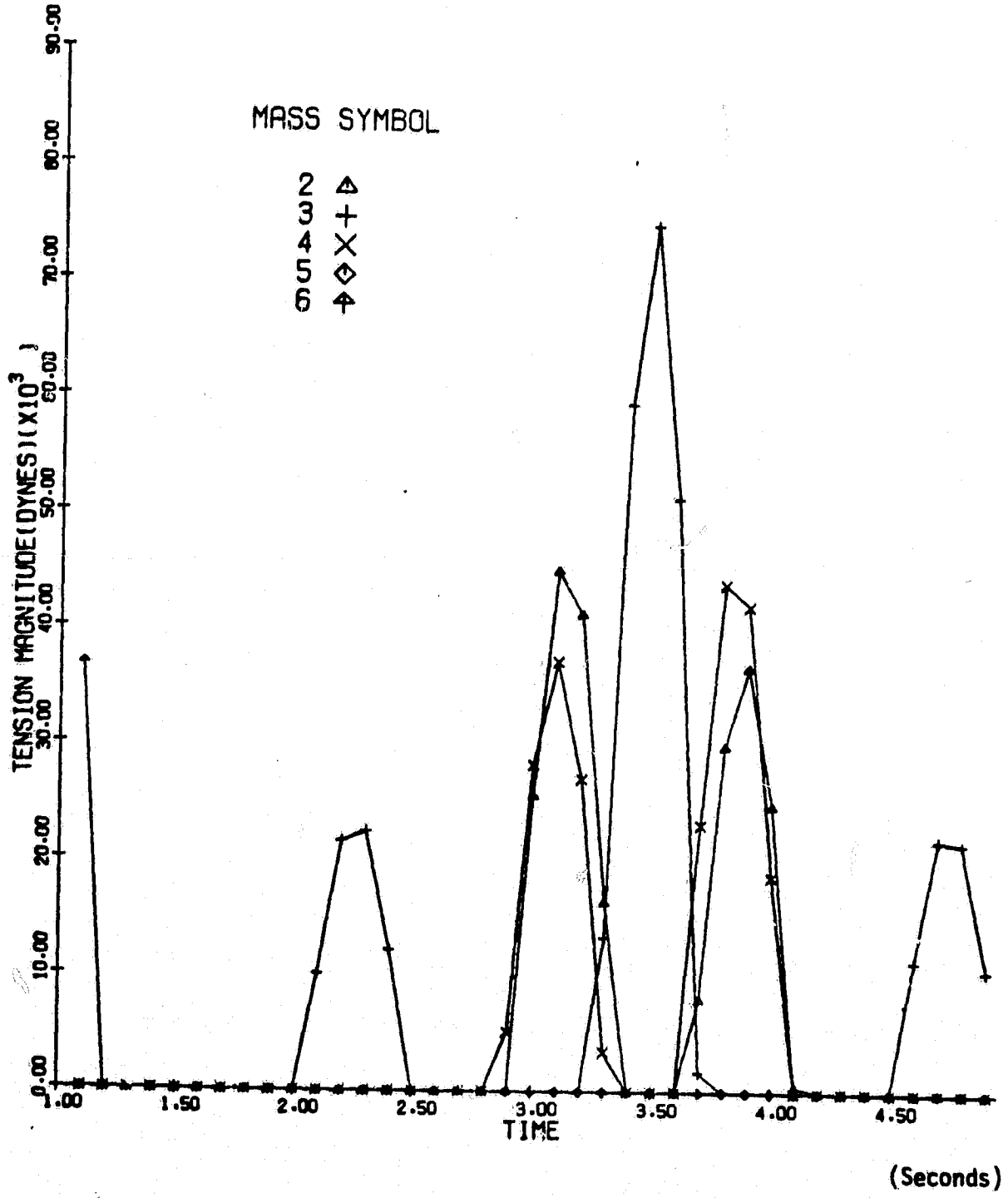

Figure 7. Tension vs. time 10 km tether cut at 5 km - expanded scale.

(a)

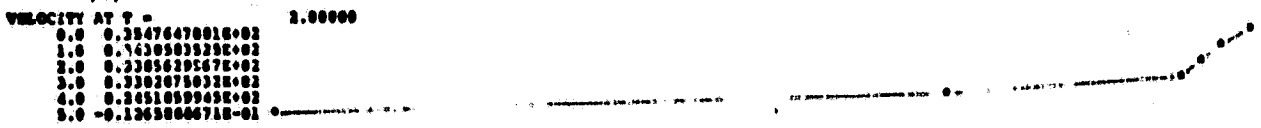

(b)

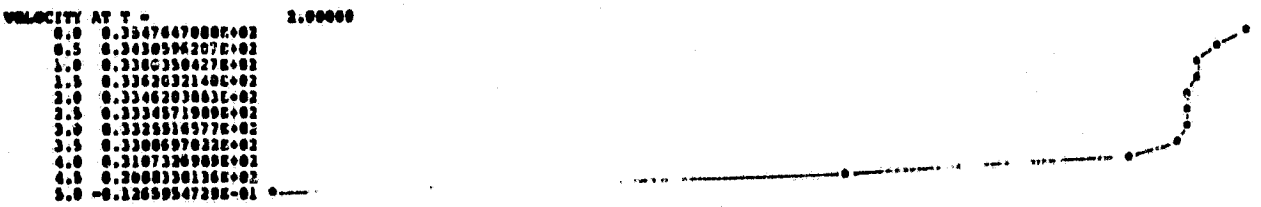

(c)

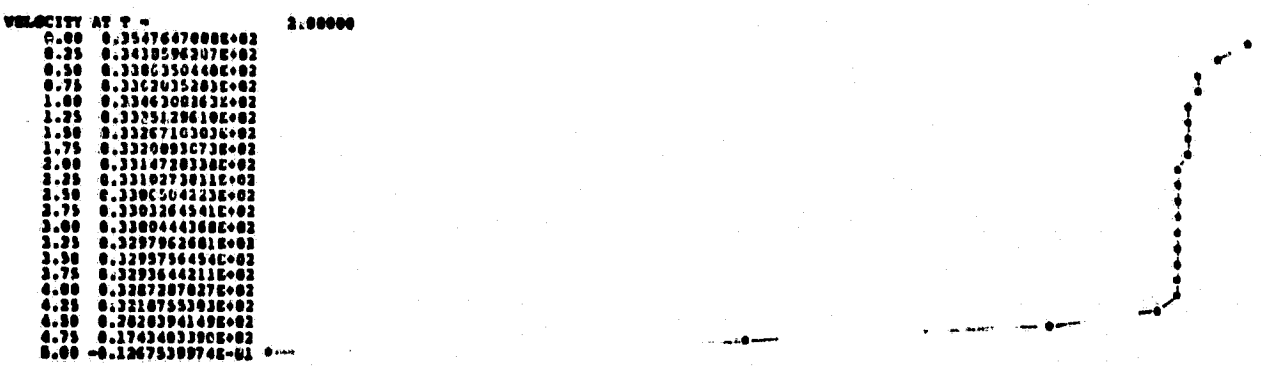

Figure 8. Velocity (cm/sec) vs. position (km) along the tether after a break 5 km from the Shuttle. Parts a), b), and c) are with the tether divided into 5, 10, and 20 sections respectively.

of the wire are affected by discretization, especially near the Shuttle. We can infer that a nearly uniform velocity profile occurs after a wire break when there is no internal damping.

3.3.2 With Damping

Sets of runs have been done with different spacing between the nodes and damping included to determine the accuracy obtainable with different resolutions. In Figure 9, a break in the wire 5 km from the Shuttle has been modelled with the wire divided into 20, 10, and 5 sections. The damping in each case is such that a .25 km length is "critically damped." The value of the damping parameter has been picked arbitrarily without regard to the actual physical properties of the wire. Figure 9 shows the recoil velocity of each node after the wire has gone completely slack. The broken end is at x = 0. and the Shuttle is at x = 5. kilometers. The agreement between the runs is fairly good. Comparing the results with 20 and 10 sections shows discrepancies of under 2 percent, and the results for 10 and 5 sections are within 5 percent. Figure 10 shows a similar comparison with the damping parameter 4 times greater (one km). The agreement between 10 and 5 sections is better than 3 percent.

Various runs have been done to determine how the shape and scale of the recoil velocity profile depends on the value of the damping parameter. Figure 11 shows plots of two runs which have identical shape and differ in scale by a factor of 2. In part a) the broken piece of wire is 10 km long, the damping parameter is .5 km and the nodes are at 1 km intervals. In part b), the wire is 5 km long, the damping parameter is .25 km and the nodes are separated by .5 kilometers. The numbers in part a) plotted every km are virtually identical to the numbers in part b) plotted every .5 kilometers.

3.4 Effect of Damping on Tether Behavior

A program which integrates only the longitudinal motion of the wire is used here to further evaluate the case of a broken tether but with damping taken into consideration. Loss of tension in the wire occurs in a short period of time and is not greatly influenced by orbital dynamics under certain conditions. The input to the new program consists of the wire diameter, density, length, elasticity, damping, tension (assumed uniform), and number of nodes, plus the masses

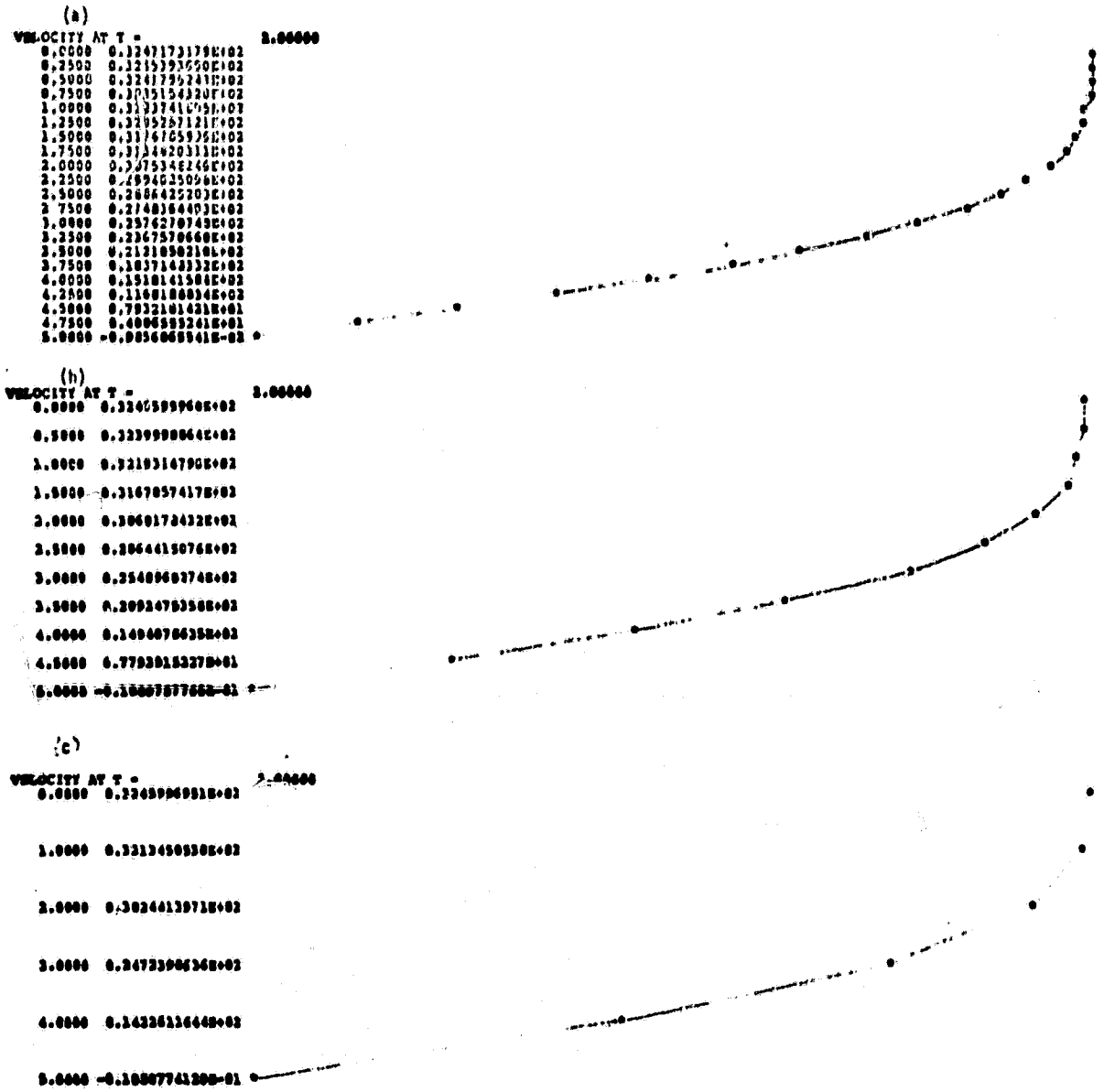

Figure 9. Recoil velocity (cm/sec) vs. distance (km) from the broken end with the wire modelled in a) 20, b) 10, c) 5 sections. The damping parameter is .25 kilometers.

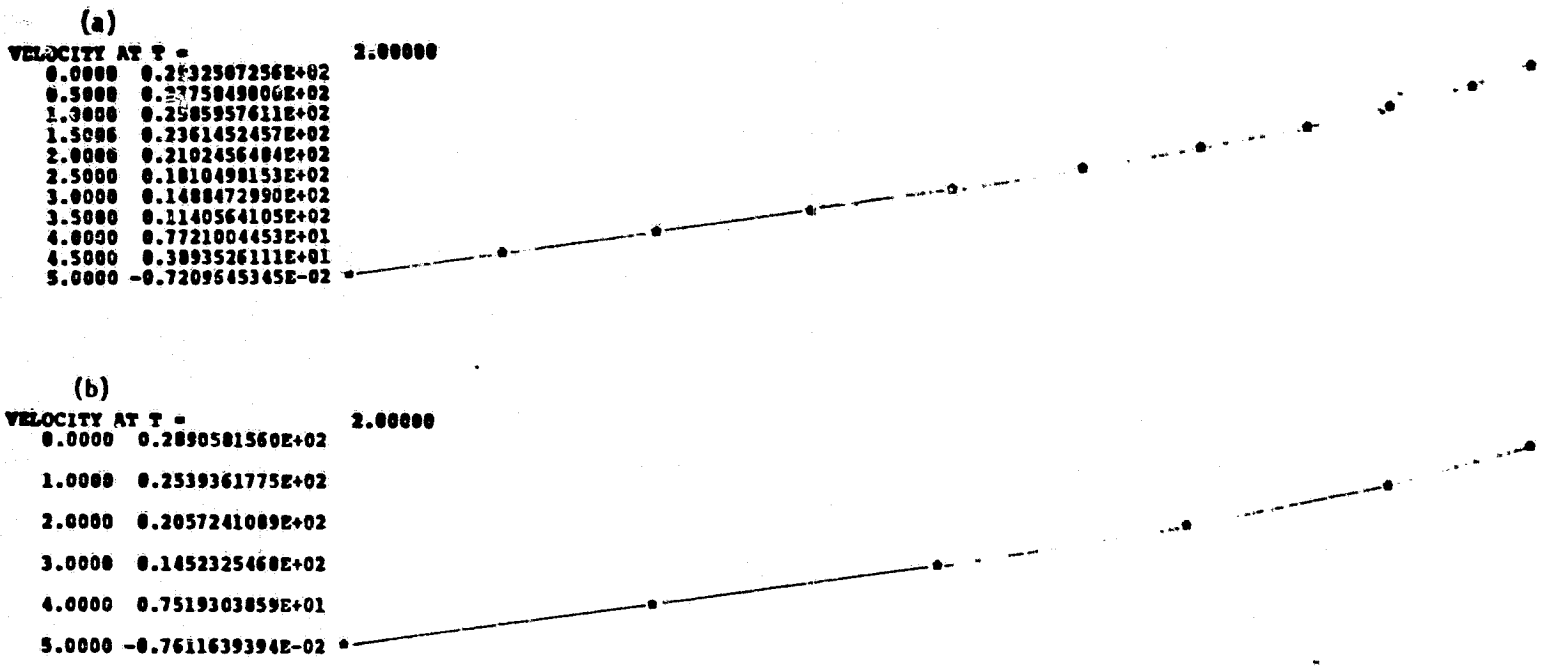

Figure 10. Recoil velocity (cm/sec) vs. distance (km) from the broken end with the wire modelled in a) 10, and b) 5 sections. The damping parameter is 1.0 kilometers.

(a)

VELOCITY AT T = 3.00000

0.0000	0.3246507036E+02
1.0000	0.3239806981E+02
2.0000	0.3218999981E+02
3.0000	0.3167405764E+02
4.0000	0.3059587848E+02
5.0000	0.2863694317E+02
6.0000	0.2548126765E+02
7.0000	0.2091552969E+02
8.0000	0.1493095801E+02
9.0000	0.7783794548E+01
10.0000	-0.2019035383E-01

(b)

VELOCITY AT T = 2.00000

0.0000	0.3246599960E+02
0.5000	0.3239998864E+02
1.0000	0.3219314790E+02
1.5000	0.3167857417E+02
2.0000	0.3060178432E+02
2.5000	0.2864415076E+02
3.0000	0.2548960274E+02
3.5000	0.2092475358E+02
4.0000	0.1494078635E+02
4.5000	0.7793915227E+01
5.0000	-0.1009757765E-01

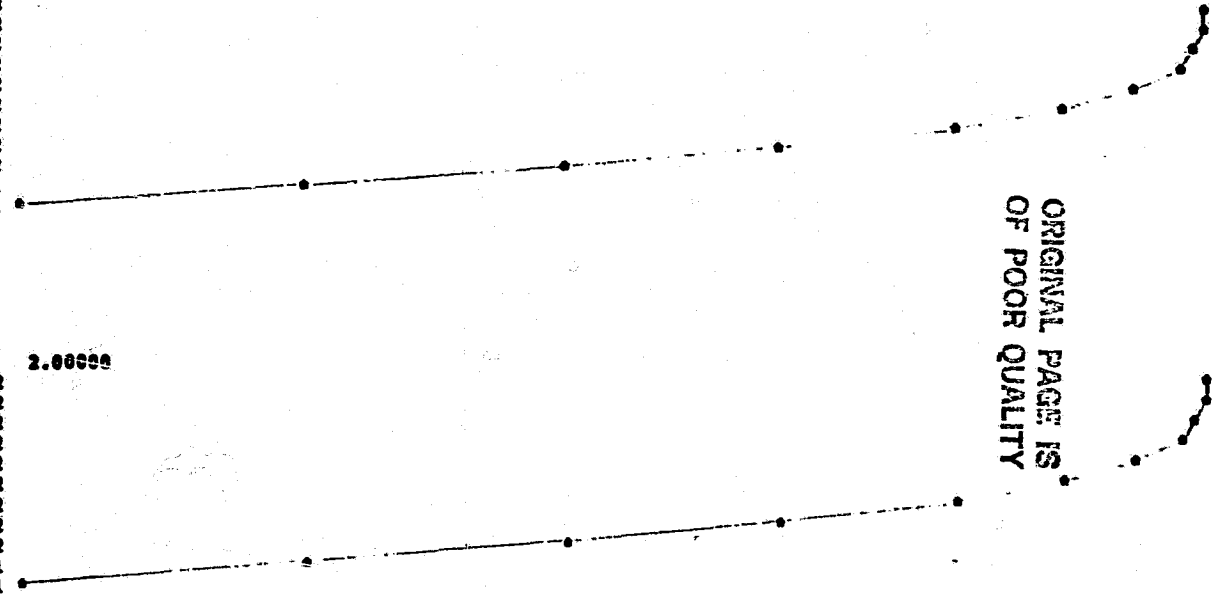

Figure 11. Recoil velocity (cm/sec) vs. distance from the broken end a) for a 10 km piece of wire with the damping parameter set to .5 km, and b) for a 5 km piece of wire with the damping parameter set to .25 kilometers.

of the Shuttle and subsatellite. The natural length of each segment is computed to give the specified tension. No other forces are currently modelled. The program integrates the one-dimensional position and velocity vs. time.

In the simulation, each section of wire has a mass m_i, elasticity k_i, and damping coefficient b_i. The damping force is of magnitude $b_i l_i$ where l_i is the length of the segment. If a mass m_i is connected to a fixed support by a spring of stiffness k_i the critical damping coefficient is $b_c = 2\sqrt{m_i k_i}$. We would expect to see significant effects in the simulation if the damping in each section is on the order of b_c. Since the mass m of each section is $m_i = A\rho l_i$ and the stiffness is $k_i = EA/l_i$ where A is the cross section, ρ is the density, and E is the elasticity, we have $b_c = 2A\sqrt{\rho E}$ which is independent of the length l_i of the segment. In the simulation, the value of b_i that must be used in each node model the damping losses depends on the number of nodes used. If the expansion is uniform and the rate of change of l is $\dot{l}$, then the rate of change of l_i is $\dot{l}/N$, where N is the number of segments. If the damping force F_o as a function of $\dot{l}$ is $F_o = b\dot{l}$, the damping as a function of $\dot{l}_i$ is $F_o = bN\dot{l}_i$. The damping coefficient for each segment is therefore $b_i = Nb$. Since the critical damping coefficient for a single section is independent of l_i we can compute a value l_{ic} which will make $b_i = b_c$. Substituting the expression $b_i = Nb = bl/l_{ic}$, we have the relation

$$bl = l_{ic} b_c$$

or

$$l_{ic} = lb/b_c \quad .$$

In this equation, b is the damping expressed as a function of the whole wire length l. The length l_{ic} of wire which is critically damped is proportional to the damping b. This implies that the shorter the piece of wire, the more it will be affected during recoil by the damping present in the wire. The longer the wire, the more elastic it will behave as far

as large scale motions are concerned. In terms of frequency, high frequencies will be damped faster than low frequencies.

In the one-dimensional computer program the damping on input is given as a fraction f of the critical damping coefficient b_c and this value of $b_i = fb_c$ is used in each wire segment. For comparison purposes, the damping coefficient for a reference length l_j can be computed by scaling the value b_i for a single segment using the relation $b_j = b_i l_i / l_j$.

Figure 12 shows the velocity profile with the damping set to .5 b_c in each .5 km section. For comparison purposes we note that this scales to .25 b_c for a 1 km section of wire. Using the wire parameters given earlier, the value of b_c is .831187 x 10^5 dynes per cm/second. The value used in this run is .2078 x 10^5 dynes per cm/sec for a 1 km section of wire. The velocity at the broken end of the wire is a little less than with no damping, and there is a plateau of nearly constant velocity near the broken end. The end near the Shuttle shows marked effects of damping with the velocity curving down toward zero at the Shuttle end.

A series of runs have been done with the tether length fixed at 5 km and varying the damping parameter to determine how the velocity profile depends on the damping parameter. The convention for specifying the damping on input is changed here to allow more direct physical interpretation and comparison between runs. The parameter now specifies the length of wire in km for which the damping is $2A\sqrt{\rho E}$, where A is the wire cross section, ρ is the wire density, and E is the elasticity. This value is what we have loosely called "critical damping" for a section of wire as discussed previously. This parameter is proportional to the amount of damping in the wire, whereas the damping constant between nodes is inversely proportional to the spacing between nodes. The damping to be used in the integration is computed automatically at the beginning of the program as a function of the distance between the nodes. The scale of the velocity drop-off at the Shuttle end was found to increase with the damping factor but not in a linear fashion. The scale appeared to be proportional to the square root of the damping. This dependence was confirmed by doing some sets of runs with the damping varied by a factor of four and the spacing varied by a factor of two. In Table 3a the spacing is .25 km and the damping parameter is .25 kilometers. In

Figure 12. Velocity (cm/sec) vs. position (km) along the tether with the damping set to half the critical damping coefficient for each .5 km section.

Table 3

Velocity vs. Distance From Break For Two Values Of Spacing And Damping Parameter

VELOCITY AT T = 2.00000

Distance from broken end	Velocity
0.0000	0.3247173179E+02
0.2500	0.3245393650E+02
0.5000	0.3241796243E+02
0.7500	0.3235154320E+02
1.0000	0.3223741805E+02
1.2500	0.3205257121E+02
1.5000	0.3176785996E+02
1.7500	0.3134820311E+02
2.0000	0.3075348246E+02
2.2500	0.2994025090E+02
2.5000	0.2886425203E+02
2.7500	0.2748364403E+02
3.0000	0.2576270748E+02
3.2500	0.2367570660E+02
3.5000	0.2121050210E+02
3.7500	0.1837148332E+02
4.0000	0.1518141584E+02
4.2500	0.1168188834E+02
4.5000	0.7932181421E+01
4.7500	0.4006555241E+01
5.0000	-0.9856065541E-02

(a) Damping parameter 0.25 kilometer

Distance from broken end	Velocity
0.0000	0.2932507256E+02
0.5000	0.2775849000E+02
1.0000	0.2585957611E+02
1.5000	0.2361452457E+02
2.0000	0.2102456484E+02
2.5000	0.1810498153E+02
3.0000	0.1488472990E+02
3.5000	0.1140564105E+02
4.0000	0.7721004453E+01
4.5000	0.3893526111E+01
5.0000	-0.7209645345E-02

(b) Damping parameter 1 kilometer

Table 3b, the spacing is .5 km and the damping parameter is 1 km. Part b) is the same as the second half of part a) to within about 3 percent. Table 3a is also plotted in Figure 13. The plateau of constant velocity does not quite extend down to the midpoint where Table 3b begins. Table 3b begins at about the same value as the midpoint of Table 3a. A second comparison was done with damping parameters of .125 and .5 km and the results are shown in Figure 14. Part b) is the same as the second half of part a) to within about 1.5 percent. The plateau is almost down to the midpoint of part a) in this case. The third comparison shown in Figure 15 was done with values of .0625 and .25 km for the damping parameter. In this case the plateau is practically level down to the midpoint of part a). The agreement between part b) and the second half of part a) is about .7 percent. The comparisons in Figures 13, 14, and 15 are consistent with the hypothesis that the scale of the velocity drop-off is proportional to the square root of the damping in the wire. In Table 3 the length and damping in a are a factor of 2 larger than in part b) and the scale differs by a factor of 2. Combining the results of Figures 4 through 6, we can infer that the scale is proportional to the square root of b x l, where b is the damping and l is the length of the wire.

The dependence of the scale factor of l suggests that something may be happening with time as the loss of tension propagates down the wire. The best run to use for studying this possibility is the run where the damping parameter is .0625 km and the wire is divided into 40 sections. In Figure 16, the tension vs. position along the wire is plotted at .2, .4, and .6 seconds after the break in the wire. The width of the tension pulse seems to be increasing with time. We can obtain a measure of the pulse width by computing the slope at the midpoint of the tension wave in each curve. Table 4 lists the tension difference at the point of maximum slope of each curve and the interval (X1 to X2) in which it occurs. The table also lists the ratio of the tension differences and the square root of the time ratio between points.

Table 4

Differences in Tether Tension vs. Time

t(sec)	X1	X2	$\Delta T*10^6$	$\Delta T_2/\Delta T_1$	$\sqrt{t_1/t_2}$
.2	0.875	1.000	.1856	1.000	1.000
.4	2.000	2.125	.130	1.428	1.414
.6	3.000	3.125	.107	1.735	1.732

It is apparent in the table that the slope is roughly inversely proportional to time and therefore the pulse width is increasing as the square root of time. This is consistent with the observation that the scale of the drop-off in recoil velocity near the Shuttle depends on the square root of the length of broken wires.

3.5 Behavior of Tether Section Nearest the Orbiter

Initial conditions have been set up with mass points at 50 meter intervals for the 200 meters of wire next to the Shuttle. The total length of the tether is 100 km with 300 kg at the upper end. The wire is 2 mm in diameter with a density of 1.5 g/cc. The equilibrium tension is about 12 kg. From previous results, the recoil velocity v_r is given by the equation

$$v_r = T/A\sqrt{\rho E} \quad .$$

With $E = .7 \times 10^{12}$ dynes/cm^2, v_r is about 3.8 m/sec. This formula assumes no losses in the wire. Since all parts of the wire recoil with the same velocity, the recoil of each section of the wire is initially independent of the length of the wire. The difference in behavior between a short piece and a long piece arises later as a result of the differential gravitational and coriolis forces which are proportional to the distance from the Shuttle. In a longer piece the forces on the more distant parts of the wire arrest the recoil of the whole wire. Integration of the motion of the masses representing the first 200 km of wire therefore gives the behavior not only of a 200 meter piece, but also the initial behavior of the first 200 meters of a longer wire.

Figure 13. Recoil velocity (cm/sec) vs. distance from the broken end with the damping parameter set to .25 kilometers.

(a)

VELOCITY AT T = 2.00000

0.0000	0.3248153745E+02
0.2500	0.3248117847E+02
0.5000	0.3248033096E+02
0.7500	0.3247853523E+02
1.0000	0.3247433761E+02
1.2500	0.3246404427E+02
1.5000	0.3243965803E+02
1.7500	0.3238571225E+02
2.0000	0.3227497852E+02
2.2500	0.3206357899E+02
2.5000	0.3168664468E+02
2.7500	0.3105626198E+02
3.0000	0.3006373578E+02
3.2500	0.2858736611E+02
3.5000	0.2650981546E+02
3.7500	0.2373334280E+02
4.0000	0.2020713620E+02
4.2500	0.1594437500E+02
4.5000	0.1103420126E+02
4.7500	0.5640903828E+01
5.0000	-0.1076954025E-01

(b)

VELOCITY AT T = 2.00000

0.0000	0.3201488315E+02
0.5000	0.3138921032E+02
1.0000	0.3035879258E+02
1.5000	0.2880295937E+02
2.0000	0.2661635286E+02
2.5000	0.2372608836E+02
3.0000	0.2010784692E+02
3.5000	0.1579729327E+02
4.0000	0.1089413641E+02
4.5000	0.5557261317E+01
5.0000	-0.8846128895E-02

Figure 14. Recoil velocity (cm/sec) vs. distance from the broken end with the damping parameter set to a) .125 km, and b) .5 km.

(a)

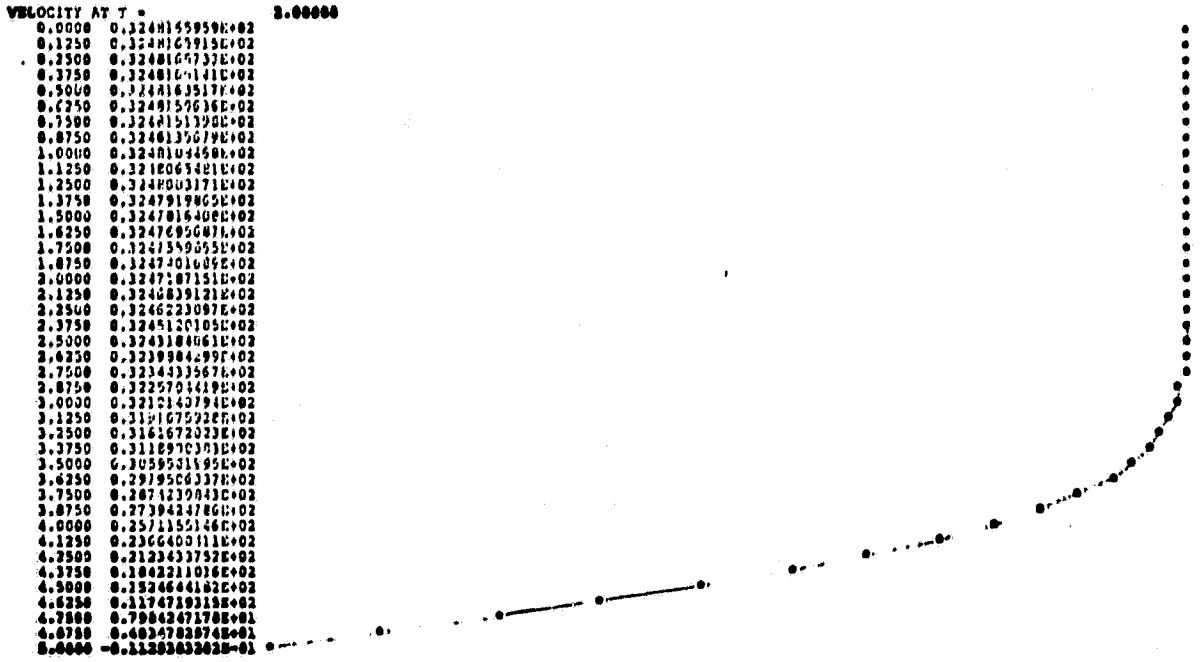

(b)

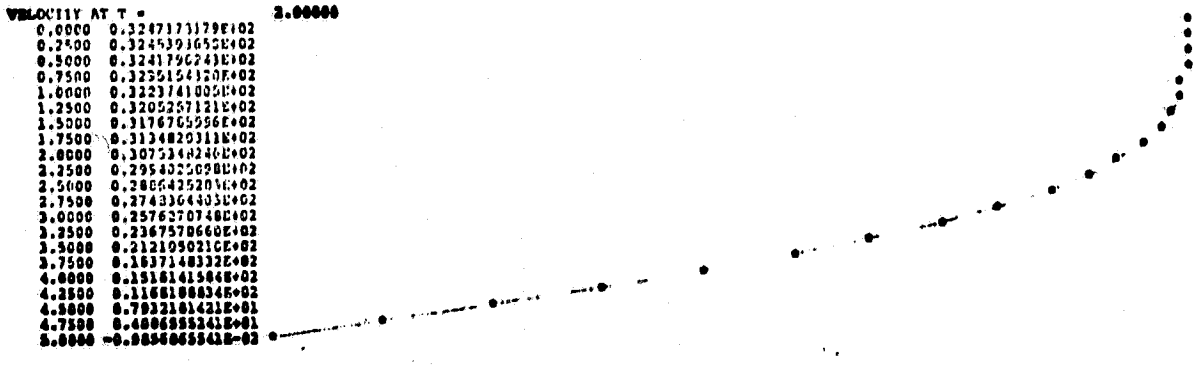

Figure 15. Recoil velocity (cm/sec) vs. distance from the broken end with the damping parameter set to a) .0625 km, and b) .25 km.

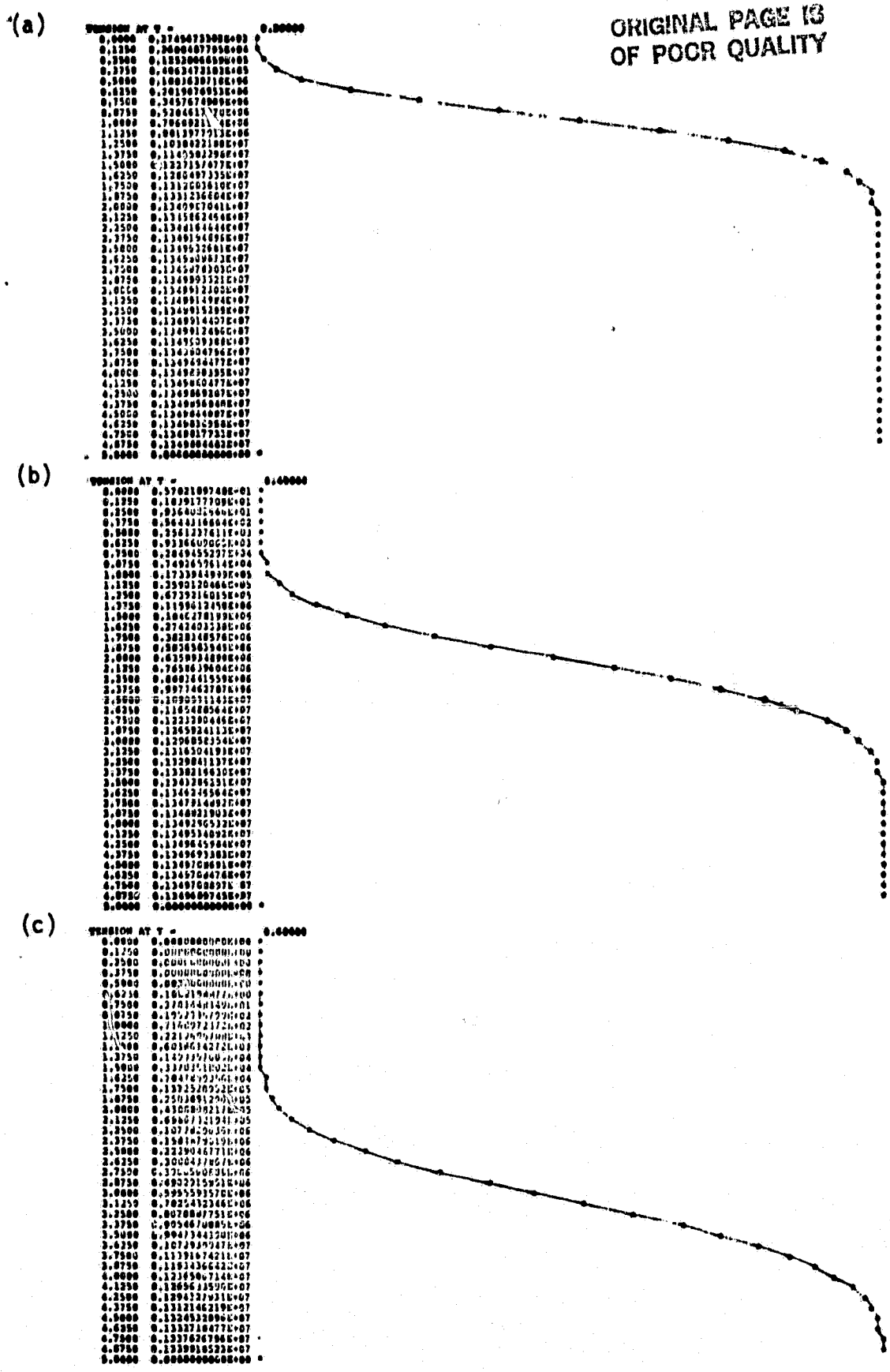

Figure 16. Tension (dynes) vs. distance (km) at a) .2 seconds, b) .4 seconds, and c) .6 seconds after the break in the wire. The damping parameter is set to .0625 km.

Figure 17 shows the behavior of the tension for each mass point plotted at .005 second intervals for the first half second. Loss of tension occurs in about .03 seconds. Figure 17b shows the radial vs. in-plane behavior for the same interval with the in-plane axis expanded to show the motion. From a tabulation of the radial displacement of each mass point vs. time, the radial velocities are computed to be about 4 m/sec. It should therefore take about 50 seconds for the end of the 200 meter wire to travel to the Shuttle.

The run has been repeated with output every half second for 70 seconds. Figure 18a shows the radial components vs. time. Figure 18b shows the in-plane displacement vs. time, and Figure 18c shows the radial vs. in-plane configuration at 2 second time intervals. In Figure 18a we see that the fifth mass point recoils downward until the radial position is -50 meters, at which time (33 seconds) it rebounds upward again. The fourth mass continues down until the distance between it and the fifth mass which is travelling upward reaches 50 meters. At that time (43 seconds) the velocities of the fourth and fifth points are reversed so that the fifth mass is travelling down again and the fourth mass is going up. When the first mass reaches -50 meters it rebounds up again (at 51 seconds). At 57 seconds the third and fourth masses rebound against each other so that the third mass is travelling up and the fourth mass down. At 63 seconds, the fourth and fifth masses rebound and reverse direction so that the fifth is travelling down and the fourth is travelling up.

In Figure 18b we see that the in-plane motion of the fifth mass is reversed when the vertical motion is reversed. The last mass point (number 2) arrives at the altitude of the Shuttle at about 50 seconds. At that time, the in-plane displacement is about 12 meters.

The behavior of the wire is rather coarsely represented by this simulation which has only 4 wire mass points. The recoil velocities are not exactly equal because of edge effects discussed previously. The timing of the rebounds is affected by the velocities. The point where the first recoil of a mass point occurs is equal to the spacing between the mass points.

Behavior of this kind would clearly have to be avoided in flight. First, better modelling of the wire, including actual physical properties and a higher level of discretization is necessary to better understand the actual motion of the tether. Second, tether tapering, tether damping and Orbiter avoidance maneuvers must be studied to either prevent the behavior or prevent the recoiling tether from moving back onto the Orbiter.

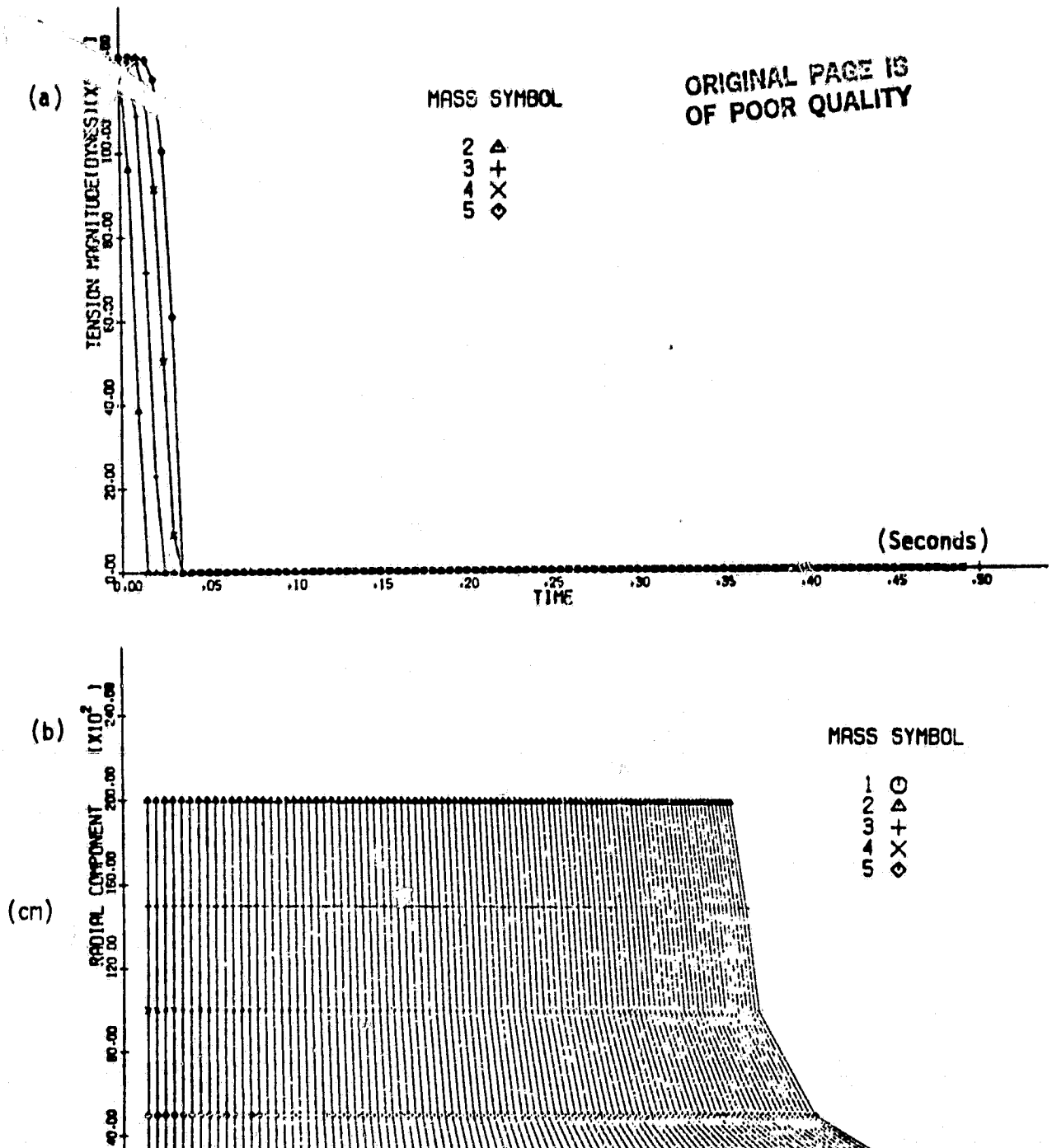

Figure 17. Recoil of the piece of wire attached to the Shuttle during the first .5 seconds after a break at 200 meters. Part a) is the tension vs. time, and part b) is the radial vs. in-plane configuration at .005 second intervals with the in-plane axis expanded to show the motion with better resolution.

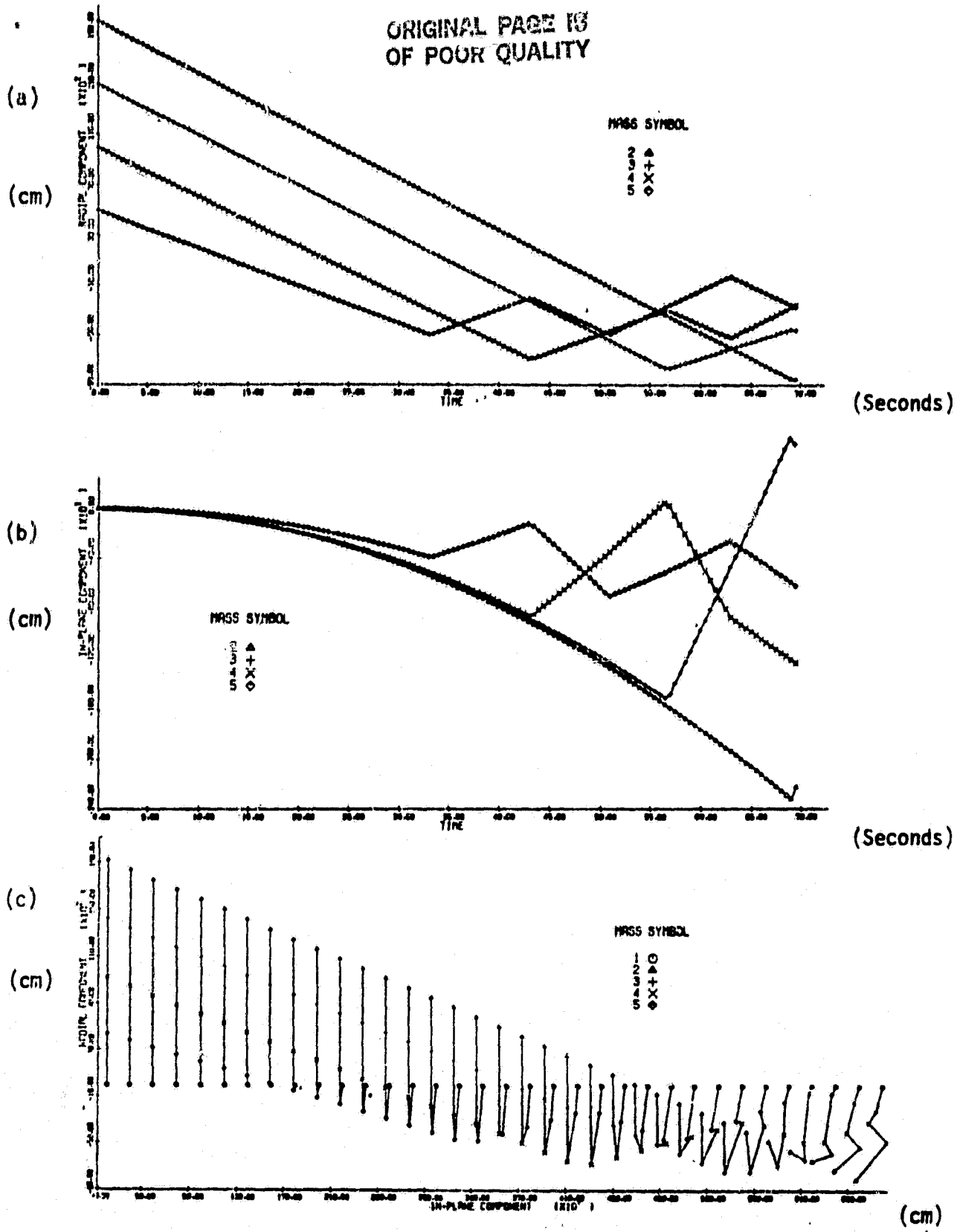

Figure 18. Recoil of a 200 meter piece of wire during the first 70 seconds after a break. Part a) shows the radial components vs. time, part b) shows the in-plane components, and part c) is the radial vs. in-plane configuration at 2 second intervals.

As a first attempt at furtner evaluation of this recoil by means of better resolution in the model, a run has been done with mass points at 20 meter intervals using a smaller program that integrates only the radial variable. The objective is to study the rebounding process that occurs in the interaction of the wire with the attachment point. Figure 19 shows the radial positions of each mass point every 10 sec. The first column is distance along the wire in km and the second column is the radial position of each mass point. At t = 0., all points are distributed at 20 meter intervals out to 200 meters. The recoil velocity acquired by each mass point is about 4 m/sec. The interaction between the masses is more complex than in the case with 5 masses. At 60 seconds we see that the first 4 or 5 points next to the Shuttle are all clustered at about 10 to 12 meters below the Shuttle which is about half the spacing between masses. The velocities of each point at 10 second intervals are shown in Figure 20. At t = 60. seconds, the velocities of the 6 points next to the Shuttle are alternating from positive to negative from point to point. The mass point at the end of the wire rebounds at about 63 seconds at a distance 56 meters below the attachment point of the wire. In the simulation with mass points at 50 meter intervals, the last mass rebounds at about 69 seconds at a point 85 meters below the attachment point. The ratio of the spacing between masses in the two simulations is 2.5, and the ratio of the lowest distances below the Shuttle in the two cases is about 1.52. The ratio of the distances is roughly the square root of the ratio of the spacing between mass points. It would be interesting to do runs with closer spacing between masses to see what effect the spacing has on the lowest point attained by the wire.

It is obvious from looking at the results that the simulations are modelling a process that is discontinuous. Most of the time, mass points are in free flight, and rebound with neighboring masses whenever the distance between mass points equals the natural length of the wire segments represented by the mass points. This type of behavior is difficult to integrate numerically at the discontinuities. It would be possible to neglect the elasticity during rebounds and treat each rebound as a point reflection. In this approximation no numerical integration is required and it should be possible to compute the behavior of a larger number of mass points by writing a program that handles only the sequencing of the rebounds, assuming free flight inbetween.

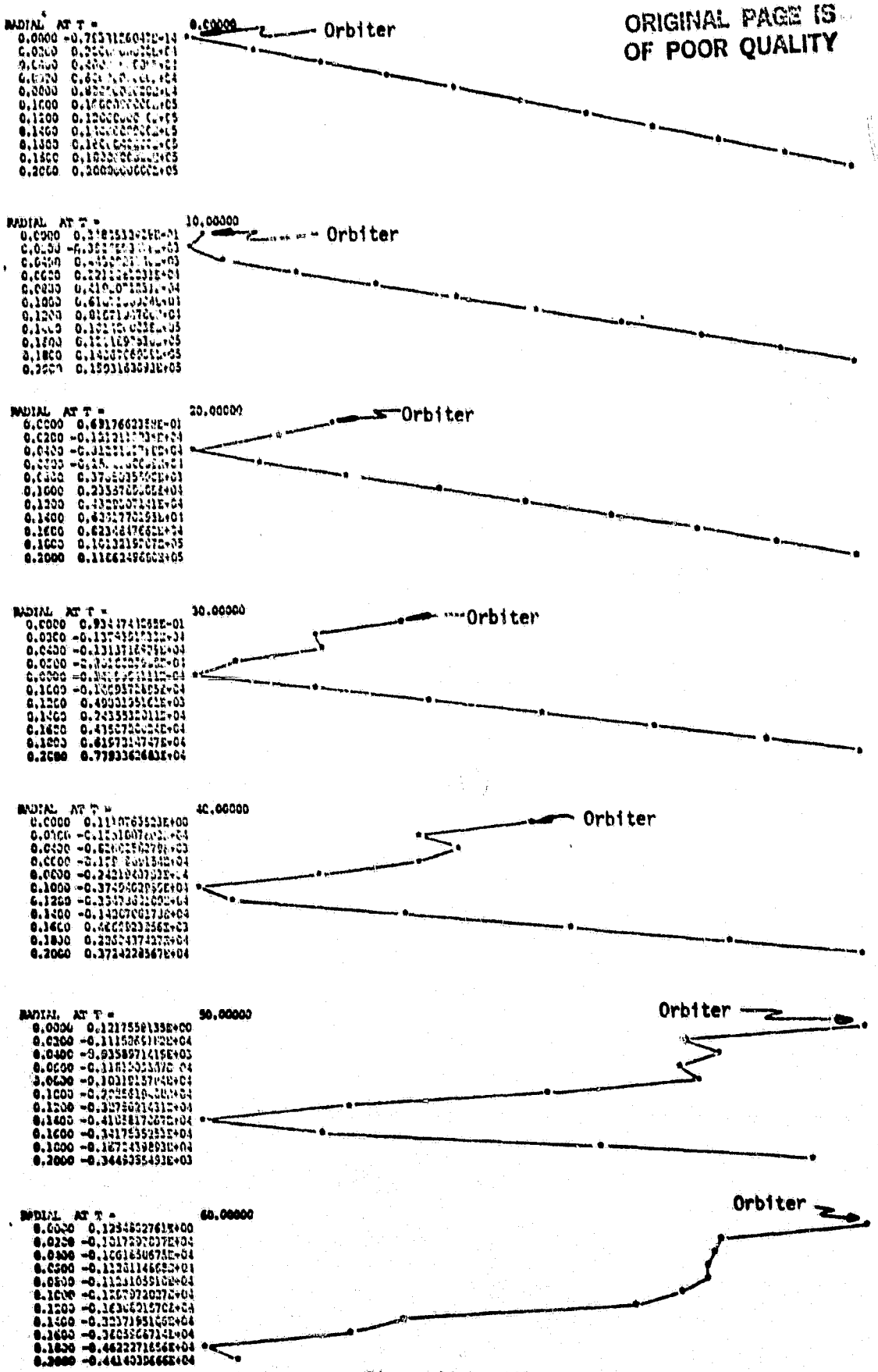

Figure 19. Radial position of each mass point after a break 200 meters from the Shuttle. The first column is the distance in km along the tether to the mass point and the second column is the radial position of each mass point.

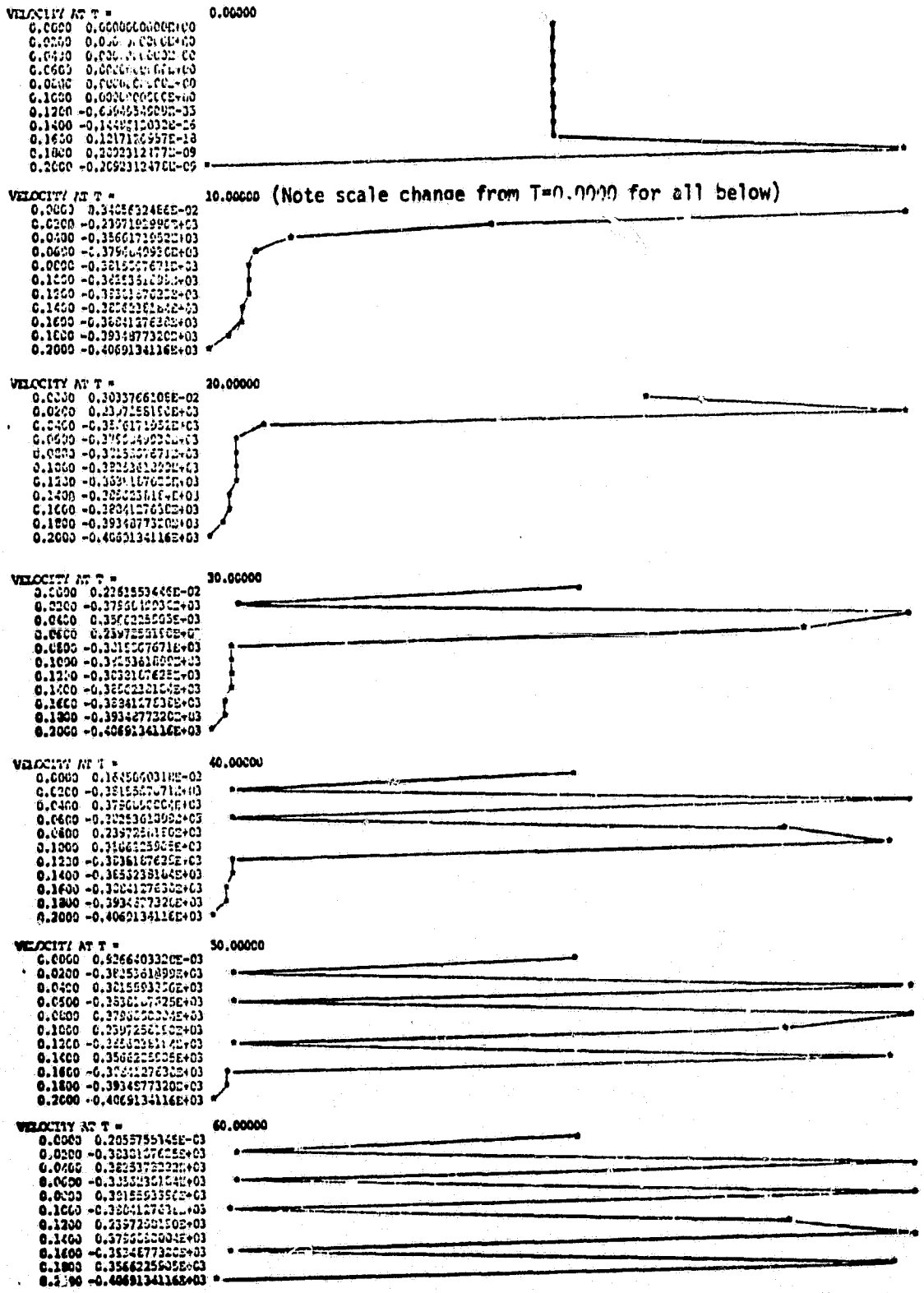

Figure 20. Velocity of each mass point in cm/sec after a break at 200 meters from the Shuttle. The first column is the distance along the tether in km to each mass point.

4.0 Tether Behavior--Reel Jam Case

4.1 Tether Modelled as Four Mass Points; Reel Jam to 10 km

One of the possible failure modes for the tether operations is jamming of the reel during deployment. In the deployment mode of the SKYHOOK computer simulation, the tension between the Shuttle and the adjacent mass representing the wire is computed from a control law rather than from the equation for stretching of an elastic wire. If the reel jams, the tension from that point on is determined by the elastic properties of the length of wire that has been deployed at that time. In order to simulate this case, initial conditions have been set up for a steady state integration (no deployment or retrieval) with the system in tension equilibrium and a radial wire velocity of 20 meters/second away from the Shuttle. To test the basic procedure, a 2 mass run has been set up with a 300 kg subsatellite 10 km away from the Shuttle on a 2 mm diameter wire. Figure 21 shows the tension as a function of time during the first 25 seconds. The maximum tension of about 160 kilograms is less than the break strength of about 850 kg for the wire (assuming the maximum allowable stress is 2.7×10^{10} subsatellite at the end of the tether is about 23 seconds. The maximum tension is reached in 1/4 of a cycle which is about 5.8 seconds. After loss of tension at about 12 seconds, the end mass goes into a free orbit. The closest approach to the Shuttle is about 5.5 km.

4.1.1 Behavior in First Five Seconds

In order to study the dynamics of the wire itself when the reel jams, a run similar to that above has been set up adding four more masses to represent the wire. A total of 6 mass points are integrated including the Shuttle and subsatellite. Figure 22 shows the tension in each wire segment as a function of time during the first five seconds as the wire is stretching. The longitudinal oscillations set up by the jamming of the reel cause the tension to vary from about 114 to 230 kilograms between the various wire segments at 5 seconds after the reel jams. It takes about 2 seconds for the tension wave to traverse the 10 km wire.

Extending this run to 25 seconds with output points every .1 second allows us to study the wire dynamics during and just after recoil. Figure 23 shows a plot of the tension in each wire segment. The tension is zero between 16 and 25 seconds. The velocity of each mass point has

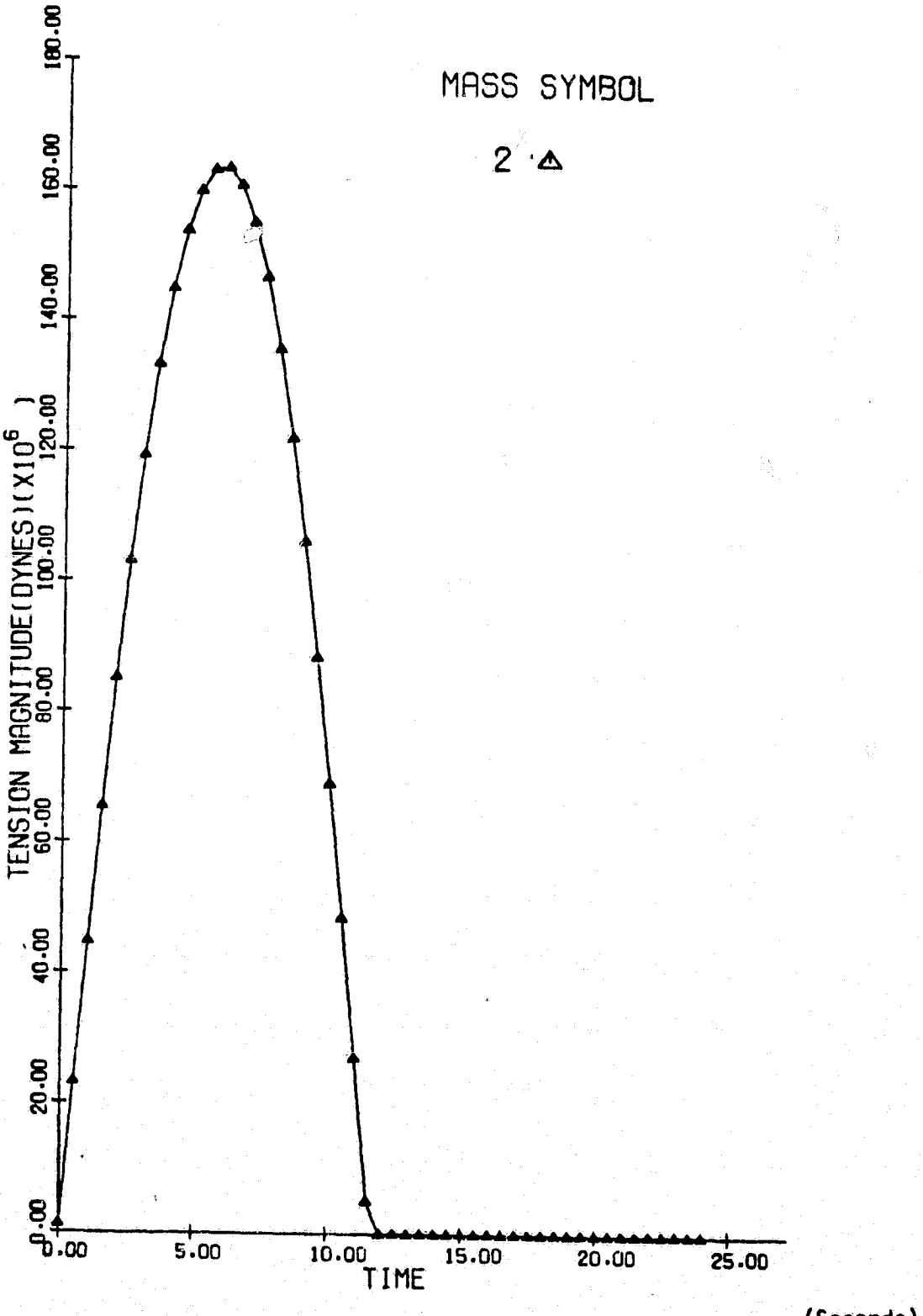

Figure 21. Tension vs. time after a reel jam - two mass model.

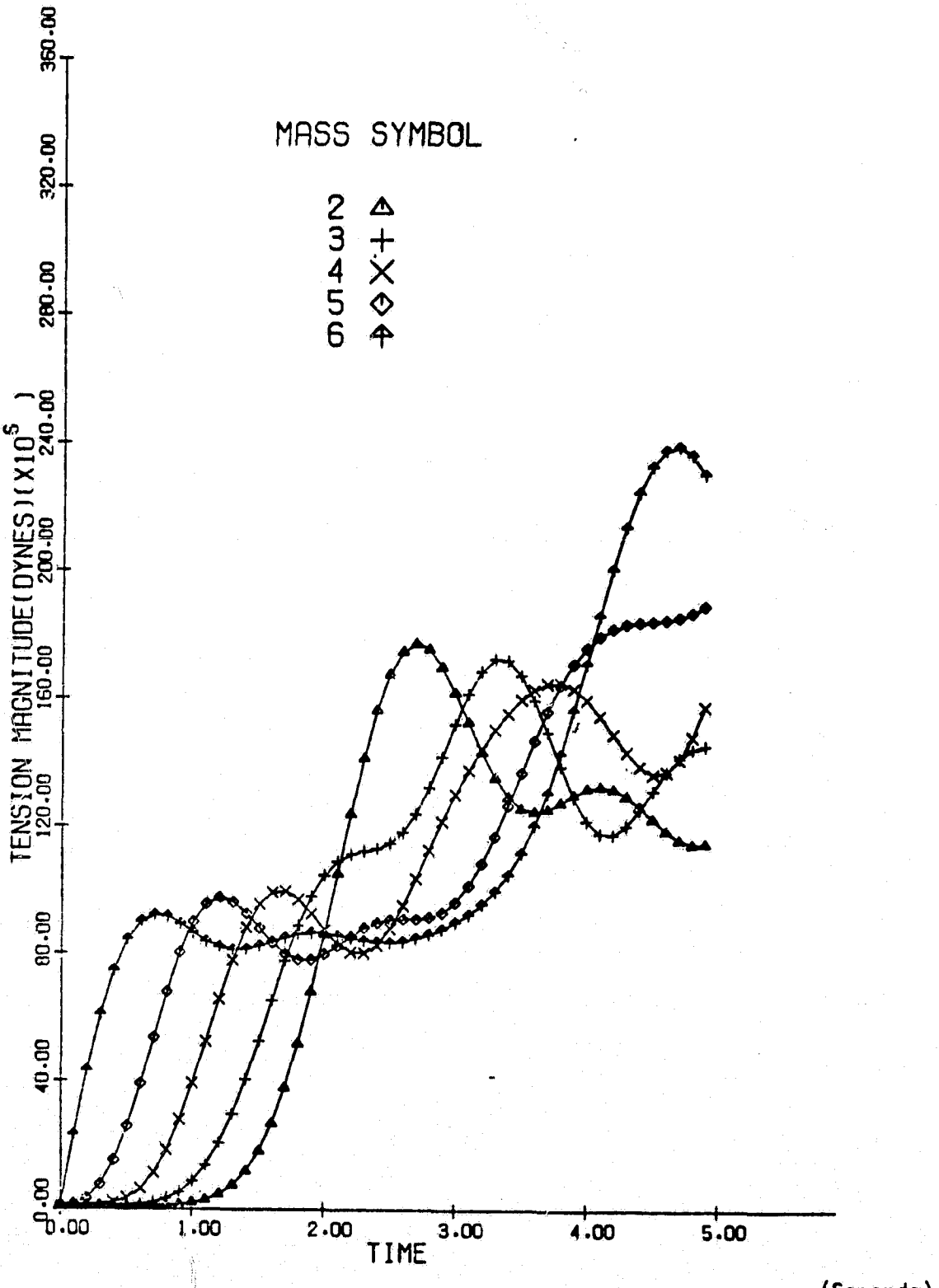

Figure 22. Tension vs. time after a reel jam - four mass model, first five seconds.

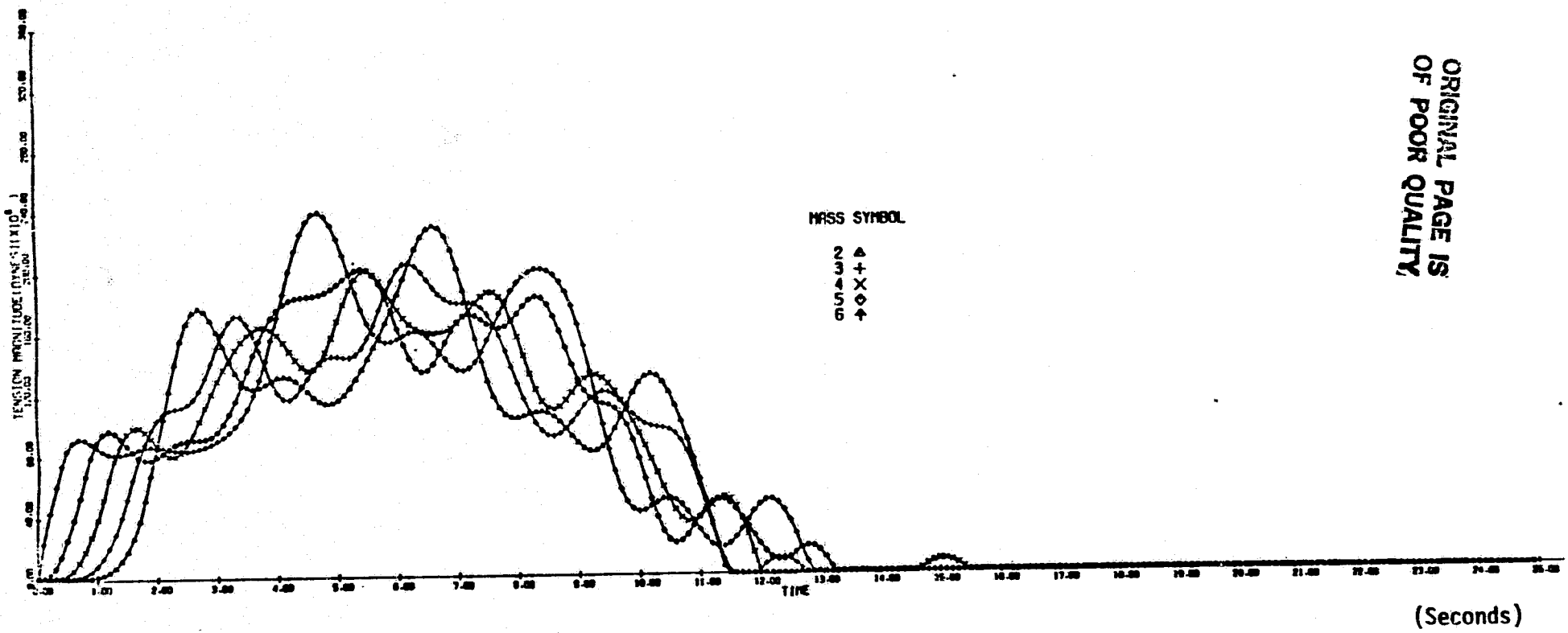

ORIGINAL PAGE IS
OF POOR QUALITY

Figure 23. Tension vs. time in each wire segment for the first 25 seconds after jamming of the deployment reel.

been computed at 16 seconds by taking the difference between successive values of the radial components. The results are given in Table 5.

Mass	Velocity	Theoretical Velocity
2	2137	2000
3	1194	1600
4	1107	1200
5	846	800
6	521	400

Table 5 radial velocity (cm/sec) just after loss of tension during recoil of the subsatellite as a result of jamming of the deployment reel.

The last column shows what the velocity would be if it was strictly proportional to the distance from the Shuttle. Aside from the oscillations along the tether caused by the jamming of the reel, the velocity is roughly in agreement with the theoretical values. The wire is contracting on itself in contrast to the behavior seen in the case of a break where the whole wire recoils with the same velocity. The four mass points representing the wire each have a mass of about 15 kg so that the 300 kg subsatellite dominates the dynamics during recoil.

Figure 24 shows the radial vs. in-plane behavior during the first 25 seconds. In the plot successive configurations at .1 second intervals are plotted to the right with a spacing of .1 inches. The orbital motion is actually to the left. The method of representation is solely one of convenience and does not reflect the orbital motion either in magnitude or sign. During the stretching period coriolis forces move the wire to the right which is opposed to the orbital motion. As the end mass recoils downward the coriolis forces are forward as can be seen in a pronounced way for the top wire section in the last configuration at the right of the plot. The horizontal axis is expanded to show the motions which are actually small (2 or 3 meters).

In order to study the oscillations set up along the wire by the jamming of the reel, the file of the radial positions for each mass point have been processed to show the relative motions between the masses graphically. The initial value of the radial component for each mass has been subtracted from the subsequent values and the plots are then

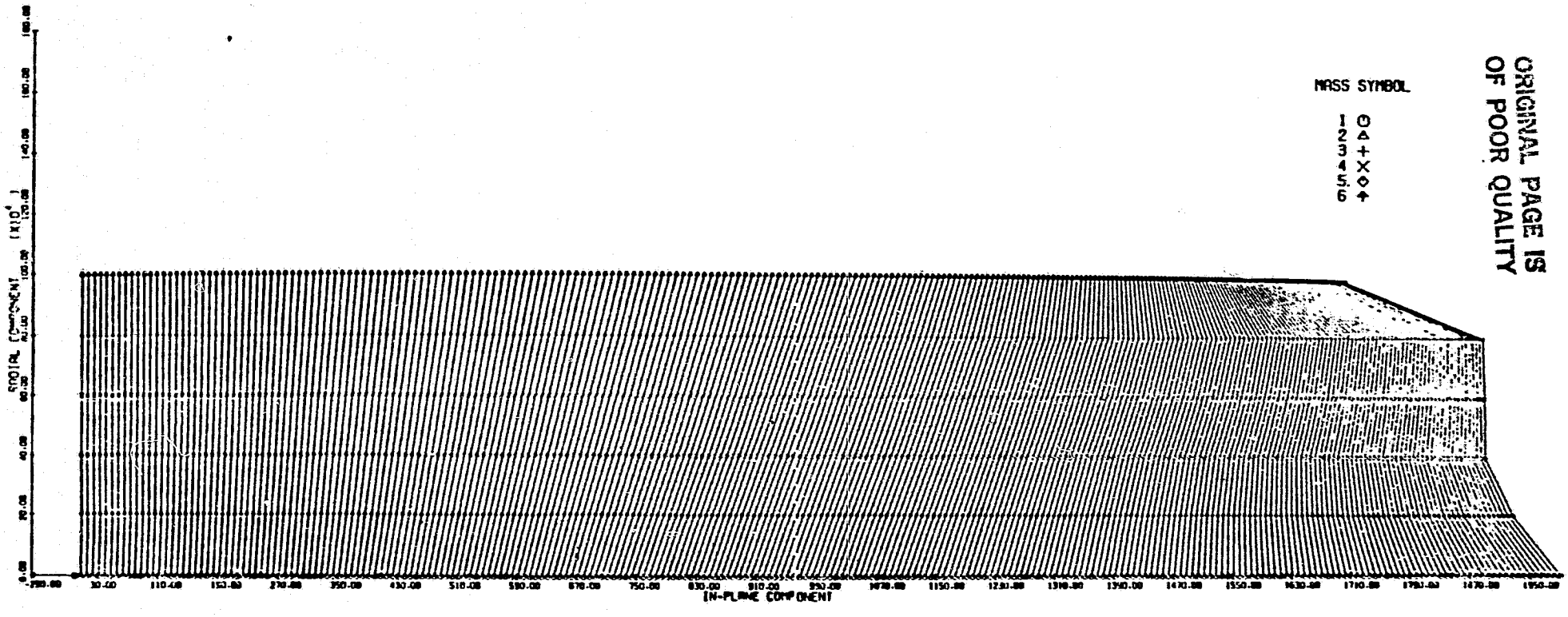

Figure 24. Radial vs. in-plane behavior during the first 25 seconds after jamming of the deployment reel.

ORIGINAL PAGE IS
OF POOR QUALITY

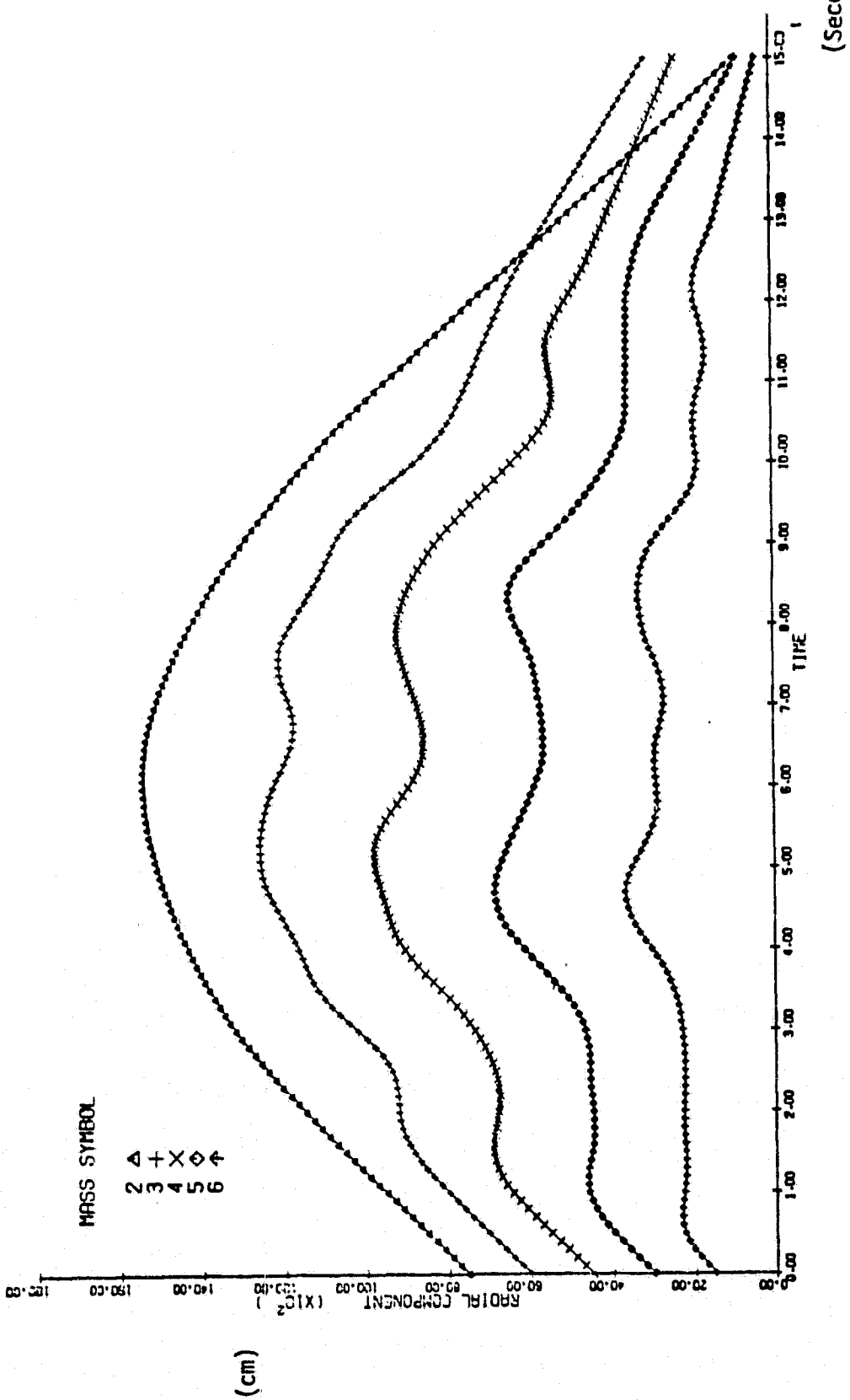

Figure 25. Radial displacement vs. time after jamming of the deployment reel. The initial value for each mass has been subtracted from each curve and the curves have been separated by 15 meters.

separated by 15 meters. This is not sufficient separation to avoid overlap of the plot for mass 2 with the plots. Increasing the separation avoids the overlap but reduces the relative amplitude of the variations in the curves. At the beginning all points are moving upward with a velocity of 20 meters/second. We can see the arresting of the upward motion starting with mass 6 and proceding up to mass 3 during the first 1.5 seconds. The motion of the 300 kg subsatellite is relatively smooth while the wire masses oscillate up and down together with a period of a few seconds. After loss of tension at about 13 seconds, the motion of the masses becomes linear. The separation between masses 4 and 5 is increasing between 13 and 15 seconds. On the tension plot (Figure 23) we see that tension is reestablished briefly between masses 4 and 5 at about 15 seconds. All masses remain out of tension from about 15 seconds to 25 seconds.

4.1.2 Behavior over 1000 Seconds

In order to see the subsequent behavior of the wire after jamming of the deployment reel, a run has been done for 1000 seconds integrating only the behavior of the Shuttle and subsatellite and neglecting wire dynamics. The in-plane vs. radial behavior is shown in Figure 26. The closest approach in the radial direction is about 5.5 km and occurs at about 450 seconds. An analytic calculation with a recoil velocity of 20 meters/sec at t = 0.0 gives a closest approach in the radial direction of 5.5 km at 439 seconds. The in-plane displacement at 450 seconds is 3.07 km in the forward direction so that the in-plane angle is about 29 degrees. The closest approach to the Shuttle is 6.1 km and occurs at about 370 seconds. At 450 seconds, the distance from the Shuttle has increased to 6.3 kilometers. Tension is reestablished at about 780 seconds as shown in Figure 27. The satellite rebounds again and the in-plane displacement decreases after rebound.

The next step in the study of this case consisted of repeating the run above with four masses added to represent the wire. Figure 28 shows the tension vs. time in the various wire segments. Unfortunately, the output interval of 10 seconds is not small enough to catch many of the points where the segments have come into tension. However, a few points do show up just before 800 seconds when the wire is reaching its maximum extension. Figure 29 shows the in-plane vs. radial behavior for the

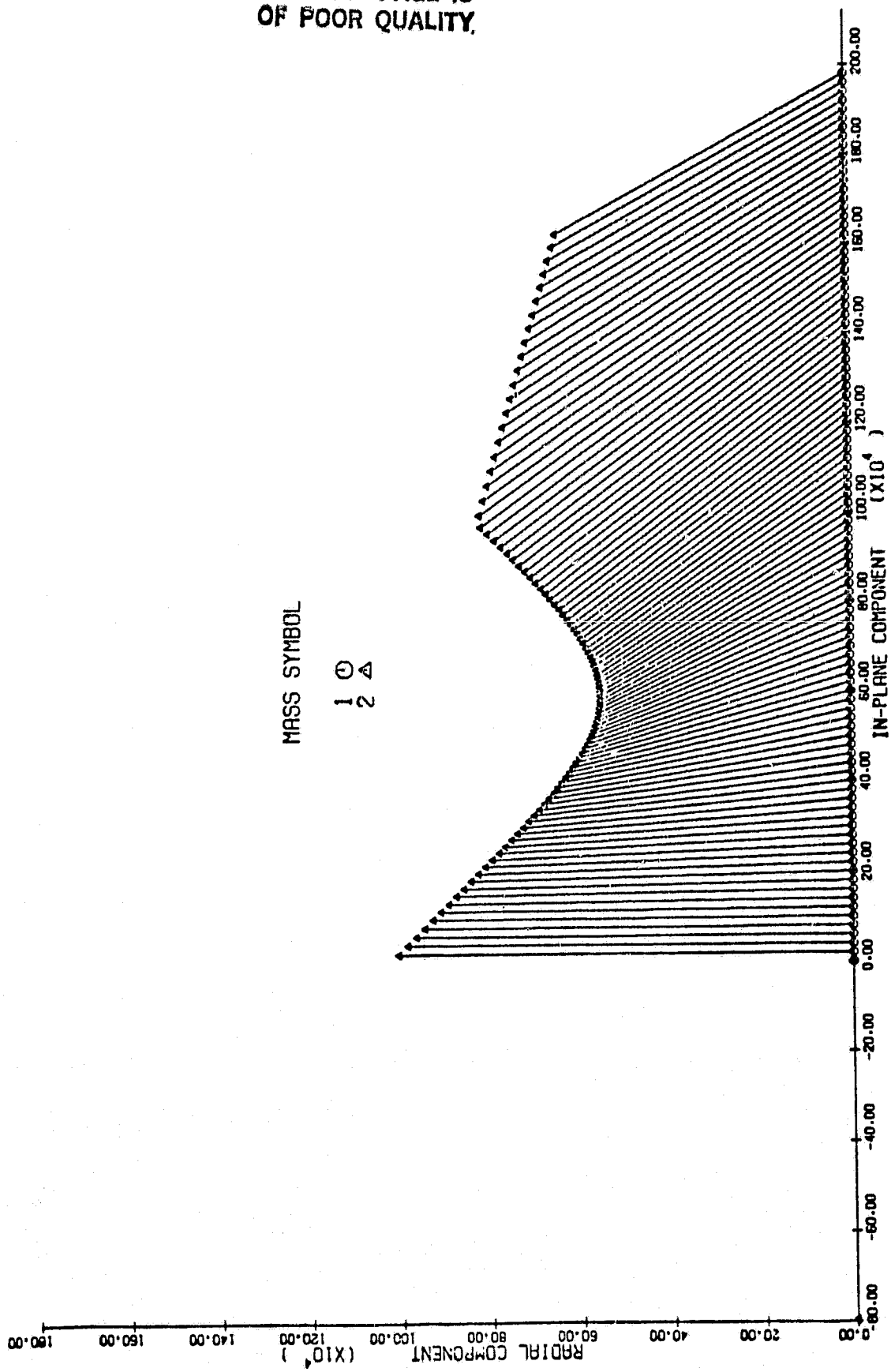

Figure 26. In-plane vs. radial behavior after jamming of the deployment reel, integrating only the motion of the Shuttle and sub-satellite. Output points are at 10 second intervals and the total time is 1000 seconds.

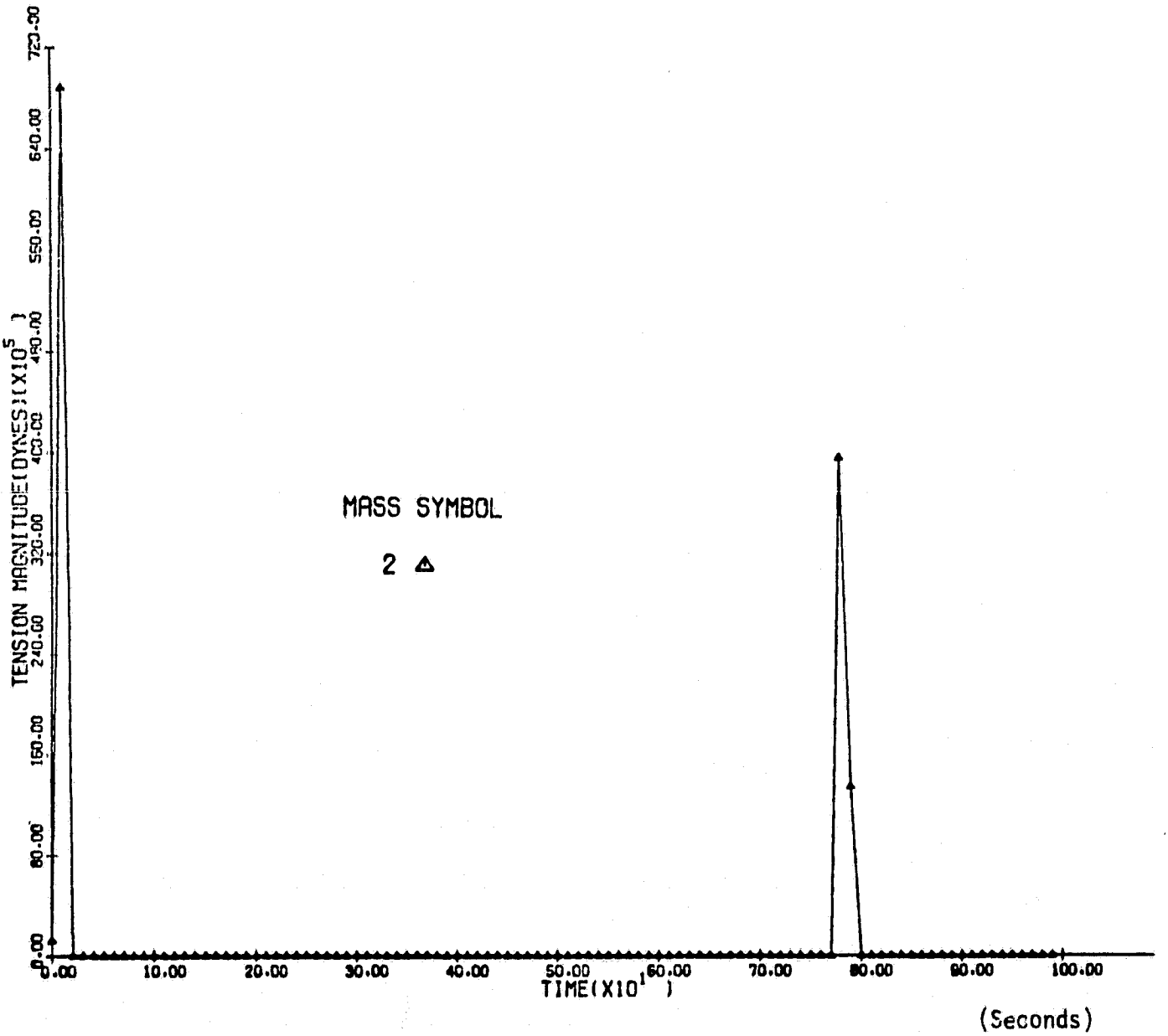

Figure 27. Tension vs. time after jamming of the deployment reel, integrating only the motion of the Shuttle and subsatellite.

ORIGINAL PAGE IS
OF POOR QUALITY

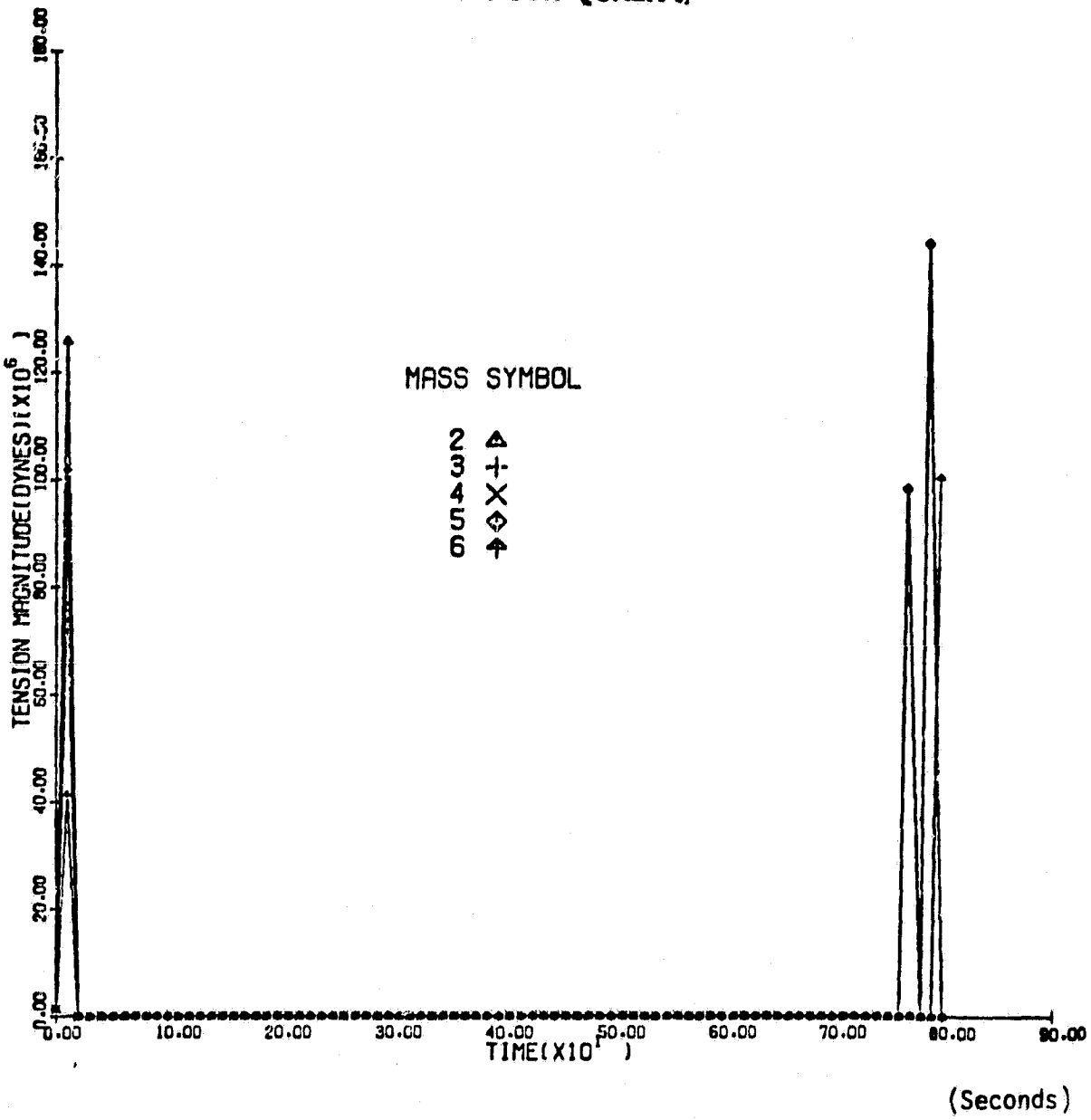

Figure 28. Tension vs. time in each wire segment with four masses representing the wire. The 10 second output sampling interval is too long to catch all the tension spikes which tend to be about one second long.

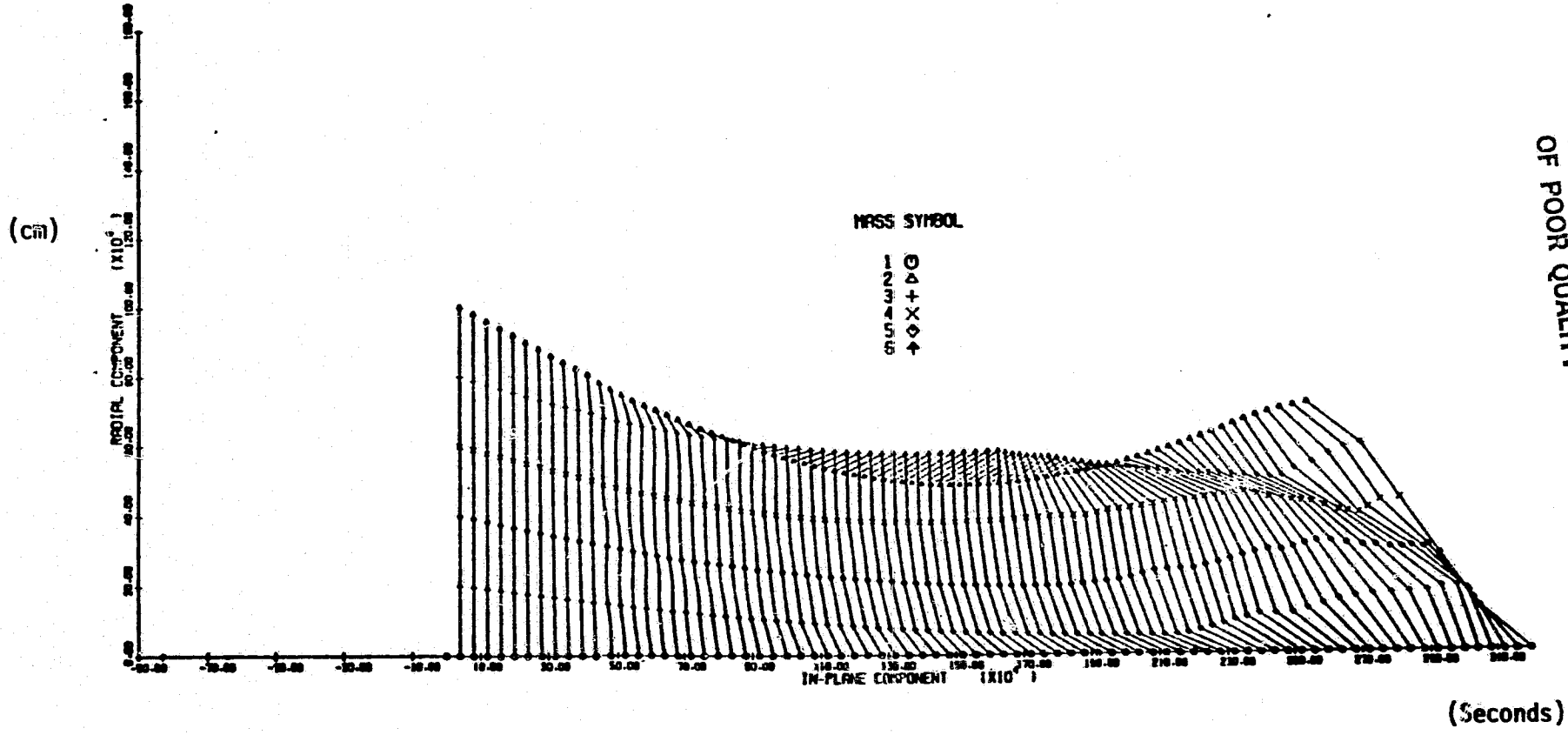

Figure 29. In-plane vs. radial behavior with 4 masses representing the wire. Output points are every 10 seconds and the total time is 800 seconds.

first 800 seconds. This Figure may be compared to Figure 26 up to the point where the wire comes back into tension at 780 seconds (Figure 26 covers 1000 seconds of orbital time). The times at which various wire segments come back into tension can in many cases be inferred from plotting the separation between each of the mass points. The natural length of each wire segment is about 2 kilometers. The smallest values of the spacings between the mass points during the first 800 seconds starting with the section next to the subsatellite are .5, 1.74, 1.56, 1.42, and .94 kilometers. The first section to regain tension is the section between masses 3 and 4, and the last section to do so is the one between mass 6 and the Shuttle. The spacing vs. time for these two sections is shown in Figure 30. Figure 30 shows the distance from the Shuttle to the subsatellite vs. time. The closest approach is 5.7 km whereas the value without wire masses was 6.1 kilometers. There is a change in slope at 780 seconds, but the wire has still not reached its maximum extension at 800 seconds.

In order to study the detailed behavior of the wire masses it is necessary to use much finer time resolution than the 10 second spacing used for these plots. Of particular interest is the behavior of the tension during rebound. The state vector at 800 seconds has been used as the initial conditions for a run covering the period 800-860 seconds with output data generated every .1 seconds. The maximum extension of the wire occurs at 807.5 seconds and has a value of 9.727 kilometers. This is less than the natural length of the wire as a result of non-straight wire configuration. Figure 32 shows the tension vs. time in each wire segment from 800 to 820 seconds. The main feature evident in the plot is that the wire never comes fully back into tension. Sections go in and out of tension in an irregular fashion. The frequency of tension spikes is greatest at the maximum extension of the wire. This behavior contrasts with the situation in Figure 23 at the beginning of the simulation when the reel mechanism jams. At the beginning the whole wire is under tension simultaneously with tension waves travelling along the wires.

4.2 Tether Modelled as Eight Mass Points; Reel Jam at 10 km

In order to see if increased resolution provides additional understanding, a run of the case described in Section 4.1 has been done with ten mass points. The mass points are separated by 1 km so that the total

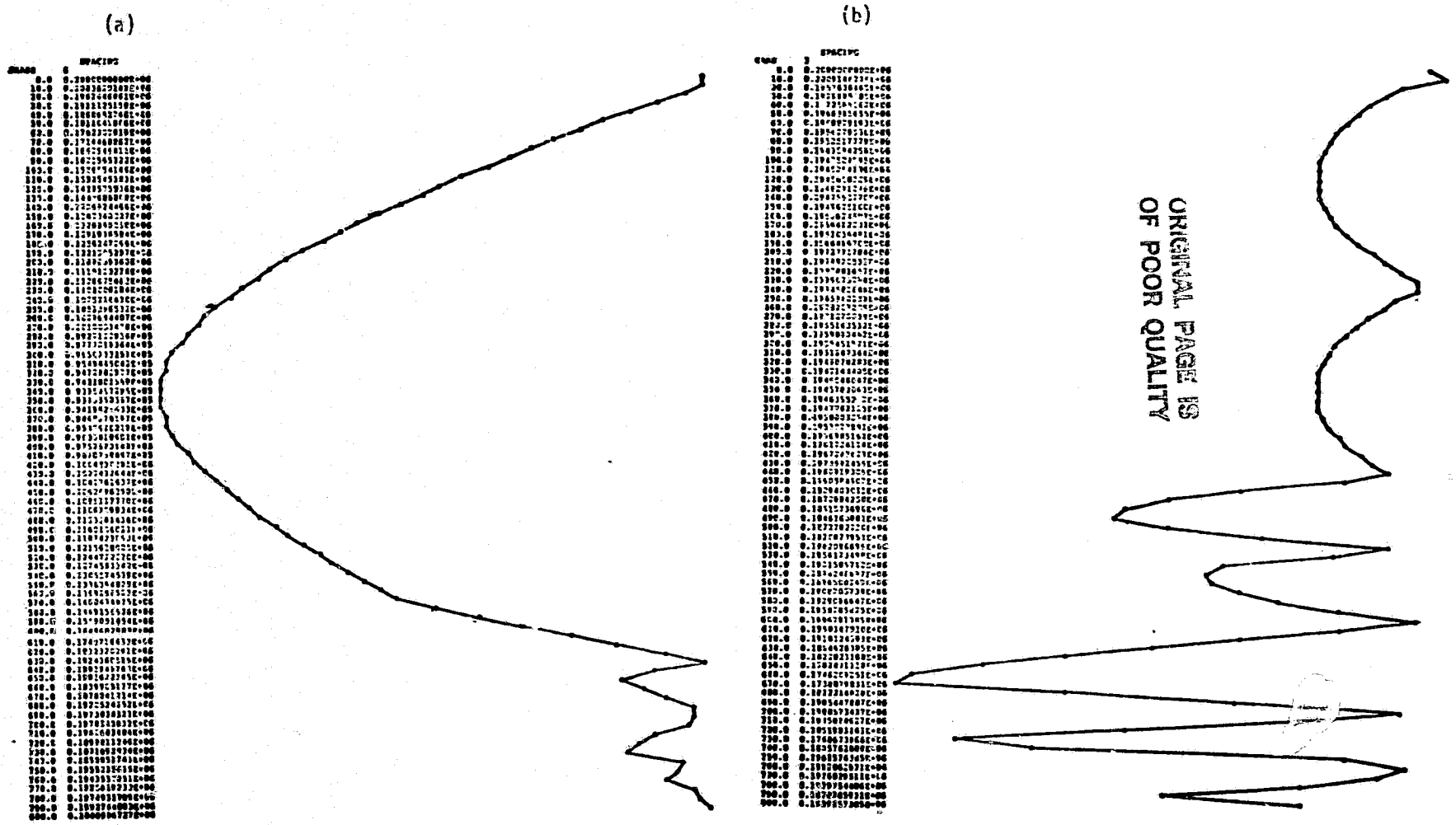

Figure 30. Spacing between mass points vs. time during the first 800 seconds after jamming of the deployment reel. There are four masses representing the wire and six masses in all. Section a) is the spacing between masses 3 and 4. Section b) is the spacing between mass 6 and the Shuttle.

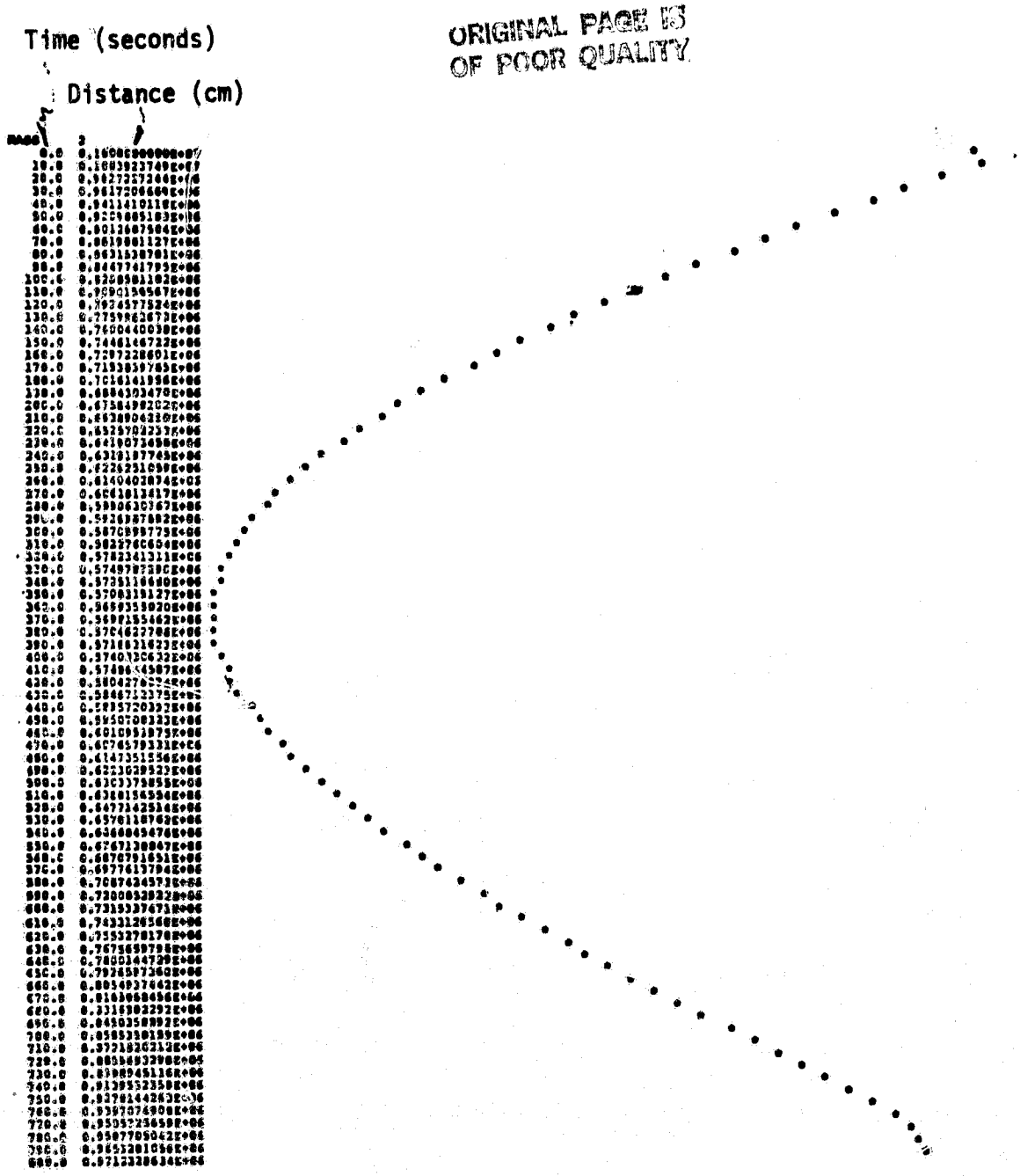

Figure 31. Distance between the Shuttle and subsatellite vs. time in the simulation with 4 masses representing the wire.

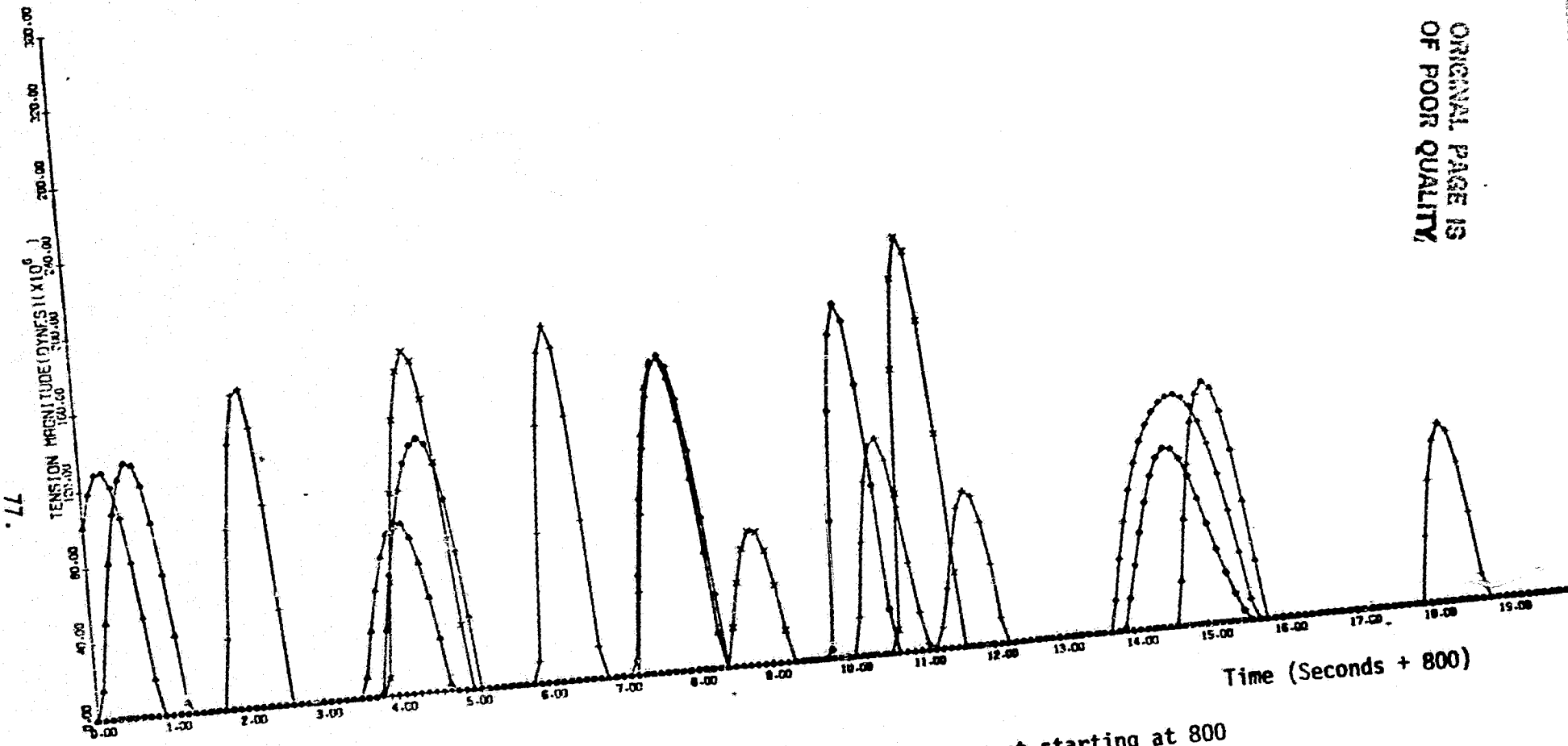

Figure 32. Tension vs. time in each wire segment starting at 800 seconds after jamming of the deployment reel.

length of wire is nine rather than ten kilometers. The subsatellite is 300 kg and is being deployed at 20 m/sec at the time of the reel jam. In the first run, the motion is integrated for 25 seconds with output points every .1 seconds. Figure 33 shows the tension vs. time in each wire segment. The results are similar to those in Figure 23. Figure 34 shows the radial vs. in-plane behavior. Comparing this Figure to Figure 24, we see some qualitative differences as a result of the increased resolution.

The case above has been continued by using the state vector at 25 seconds as the initial conditions for a run with output every 5 seconds. The run was allowed to continue for about 2 hours of computer time, at which point the program had integrated the motion for about 495 seconds of orbital time. The tension vs. time is shown in Figure 35. This plot covering the orbital time period from 25 seconds to 520 seconds may be compared to Figure 21. The scale of the vertical axis differs by a factor of 10 between the two Figures. Figure 21 shows no tension spikes in the time interval corresponding to Figure 35. The spikes shown in Figure 35 represent oscillations between the wire mass points. The wire as a whole has not reached its maximum extension. The plotting interval of 5 seconds is not small enough to catch all the tension spikes which occur. However, the spacing is half that used previously and there are more mass points so that there is an increased probability of catching tension spikes.

Figure 36 shows the radial vs. in-plane behavior for the period 25 to 520 seconds. This plot may be compared to the first part of the plot in Figure 29 which covers the time period 0.0 - 800.0 seconds with output every 10 seconds. There are qualitative differences in the behavior, particularly at the ends of the wire. The successive configurations in Figure 36 show considerable overlap with a spacing of .2 inches between configurations. Figure 37 is the same as Figure 36 with only every fifth configuration plotted to reduce the amount of overlap. Successive configurations are separated by 25 seconds.

Repeating this run with atmospheric drag and a deployment velocity of 10 m/sec gives the result shown in Figure 38 where the wire configuration is plotted every 20 seconds. Comparing this to Figure 37 we see that there is much less forward movement as a result of the lower recoil velocity which reduces the coriolis forces, and atmospheric drag which is opposed to the coriolis forces in this case. Figure 39 shows the

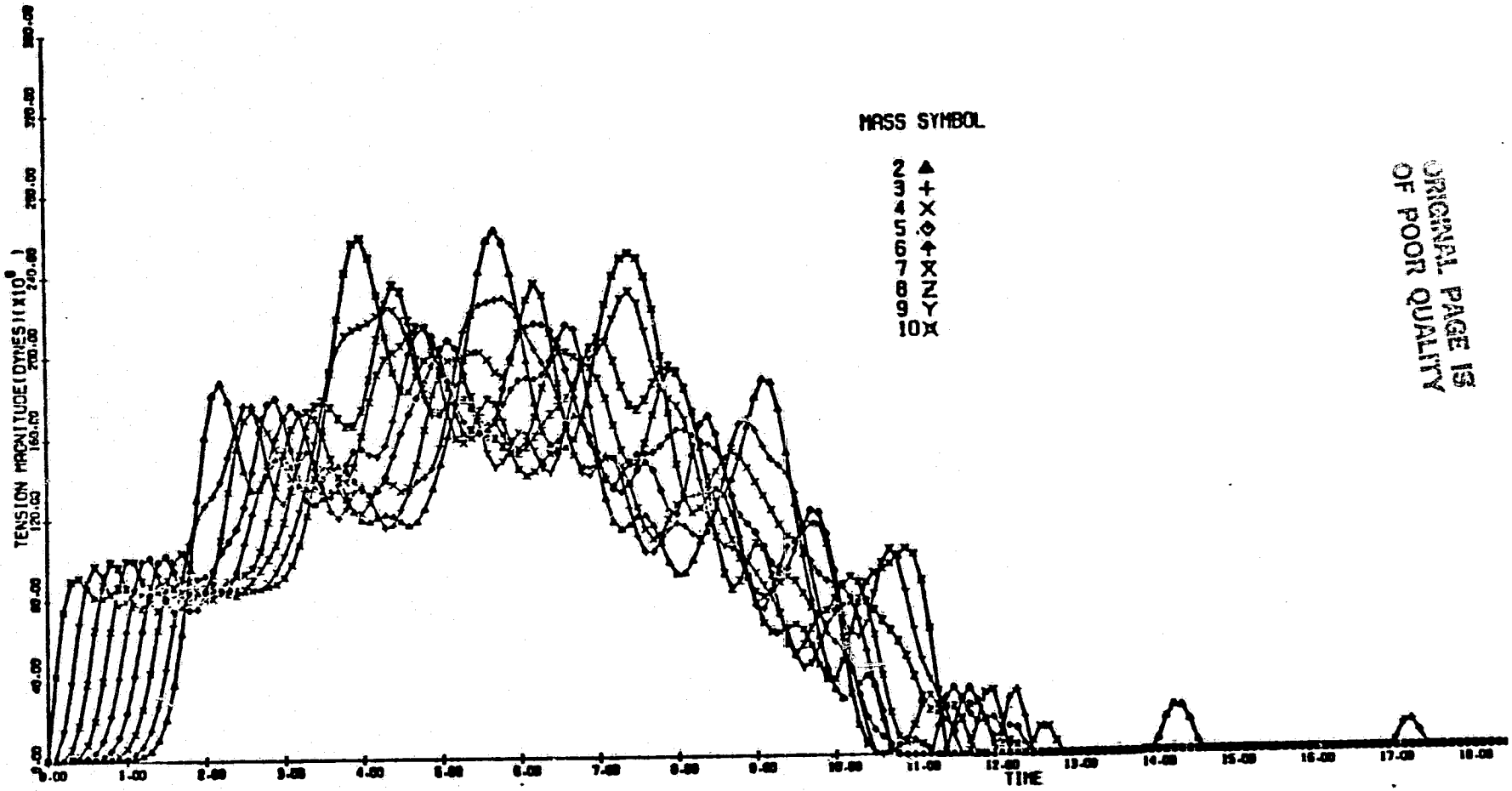

Figure 33. Tension vs. time in each wire segment for the first 18 seconds after jamming of the deployment reel. Ten mass points at 1 km intervals are used to represent 9 km of wire.

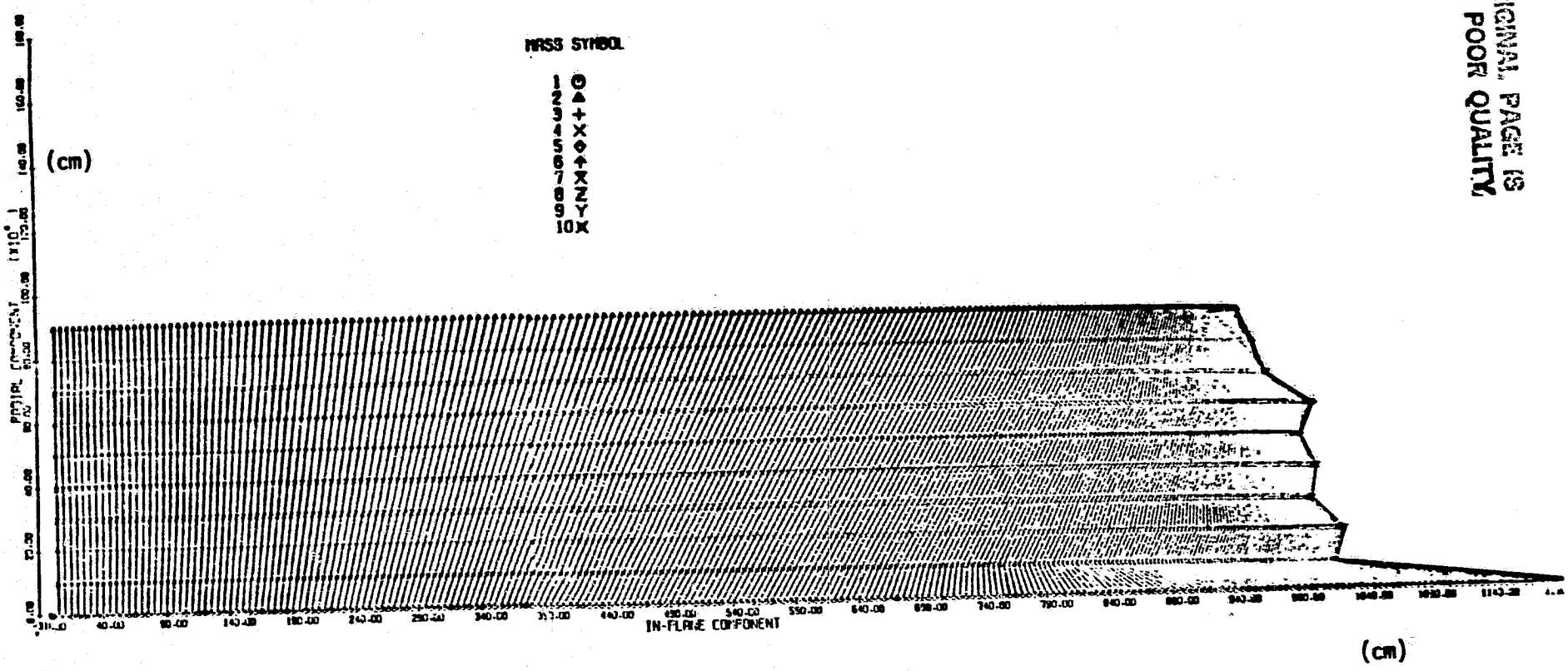

Figure 34. Radial vs. in-plane behavior during the first 25 seconds after jamming of the reel. Configurations are separated by .1 seconds of orbital time.

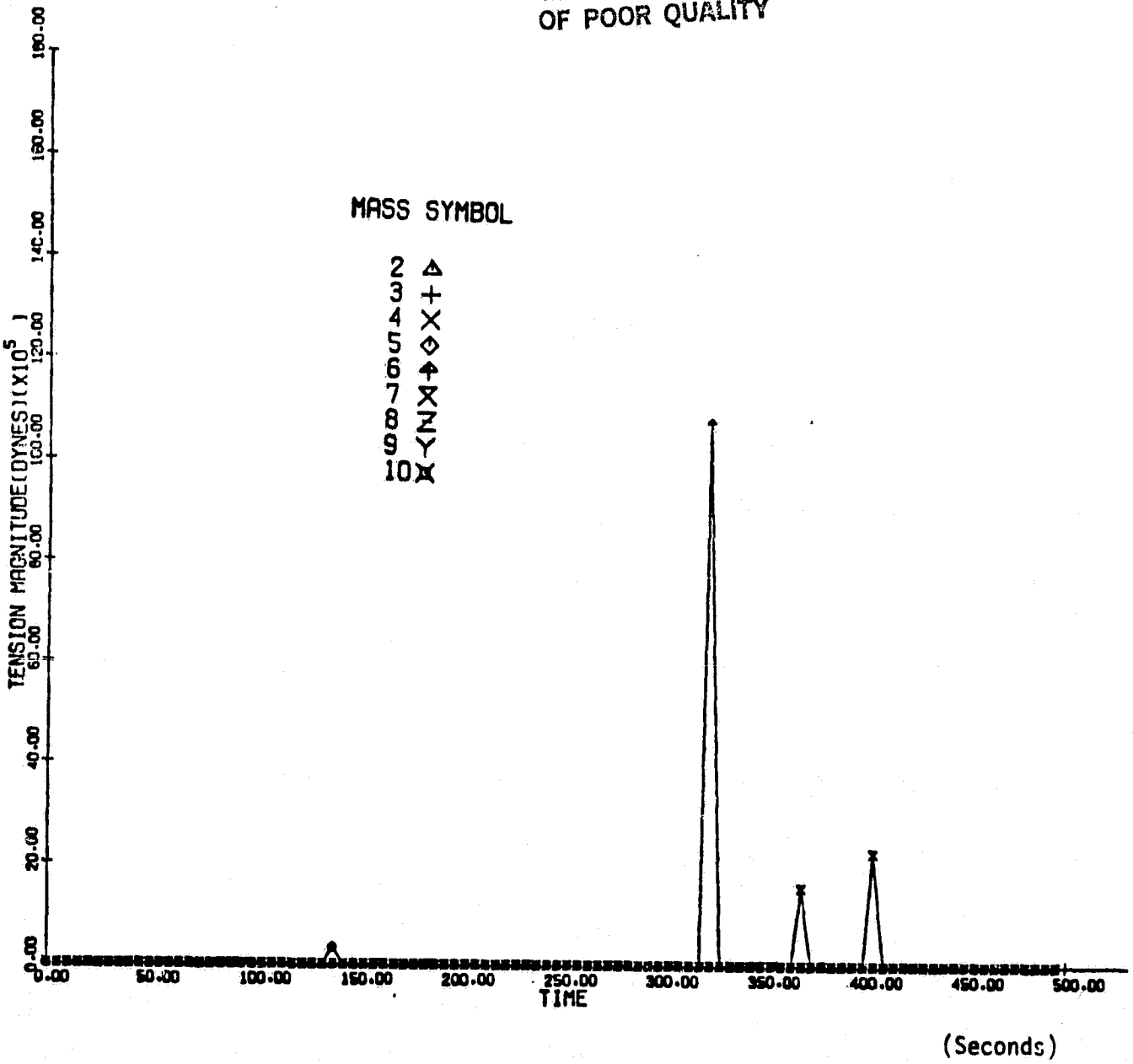

Figure 35. Tension vs. time in each wire segment after jamming of the deployment reel for the time period 25 to 520 seconds with output every 5 seconds.

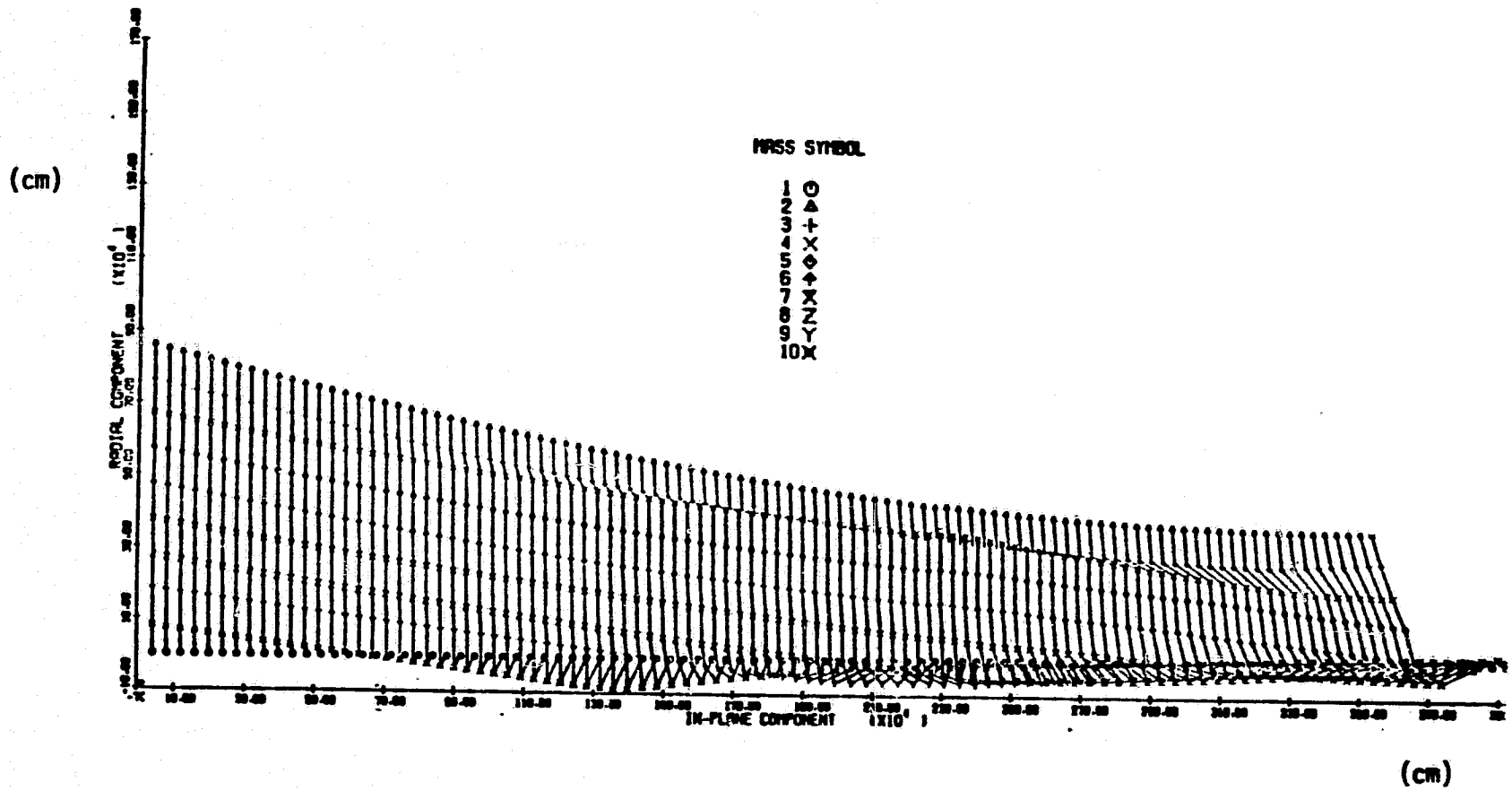

Figure 36. Radial vs. in-plane behavior for the time period 25 to 520 seconds after jamming of the reel. Output is every 5 seconds.

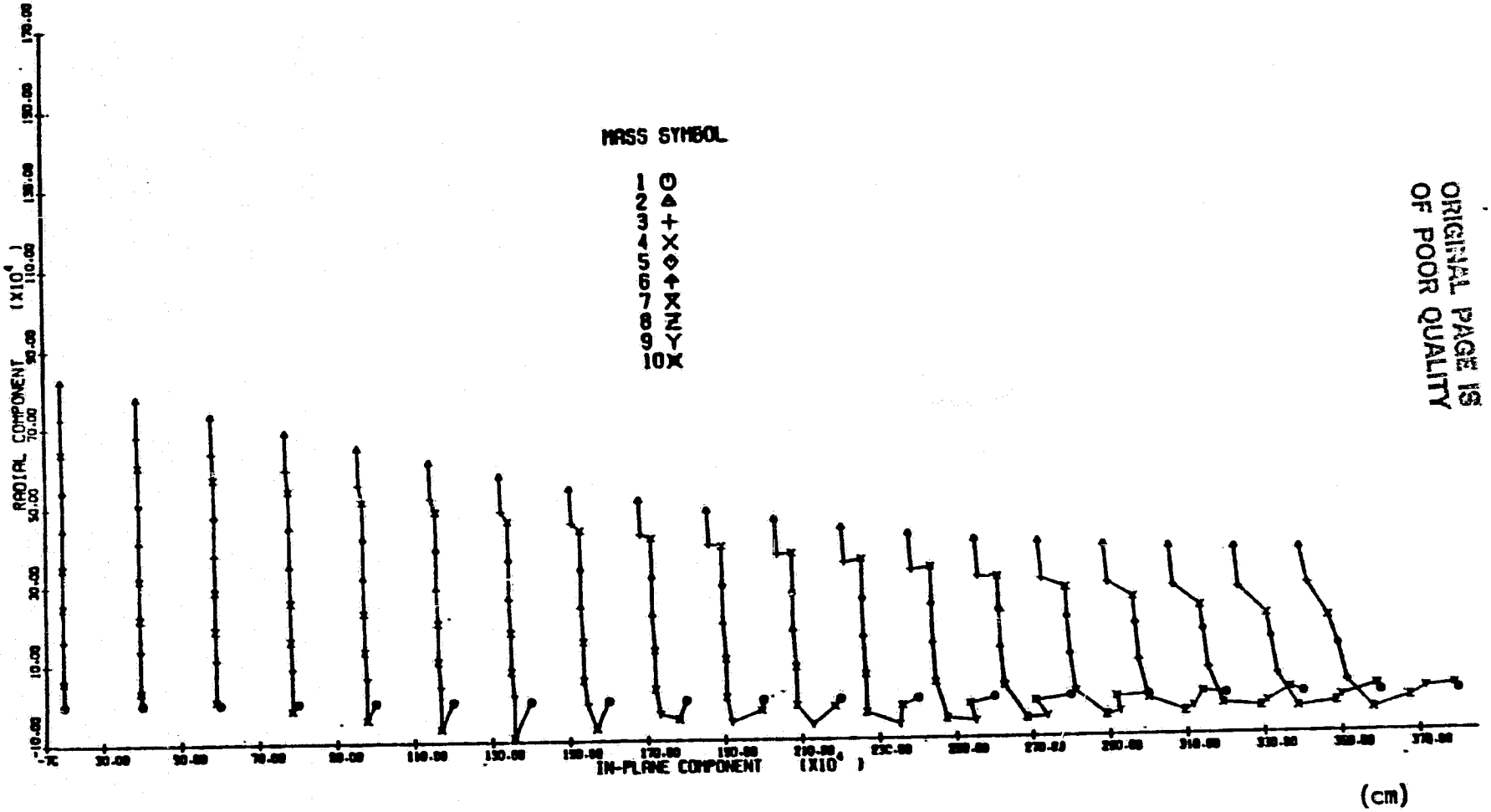

Figure 37. Same as Figure 36 with only every fifth configuration plotted. Configurations are separated by 25 seconds.

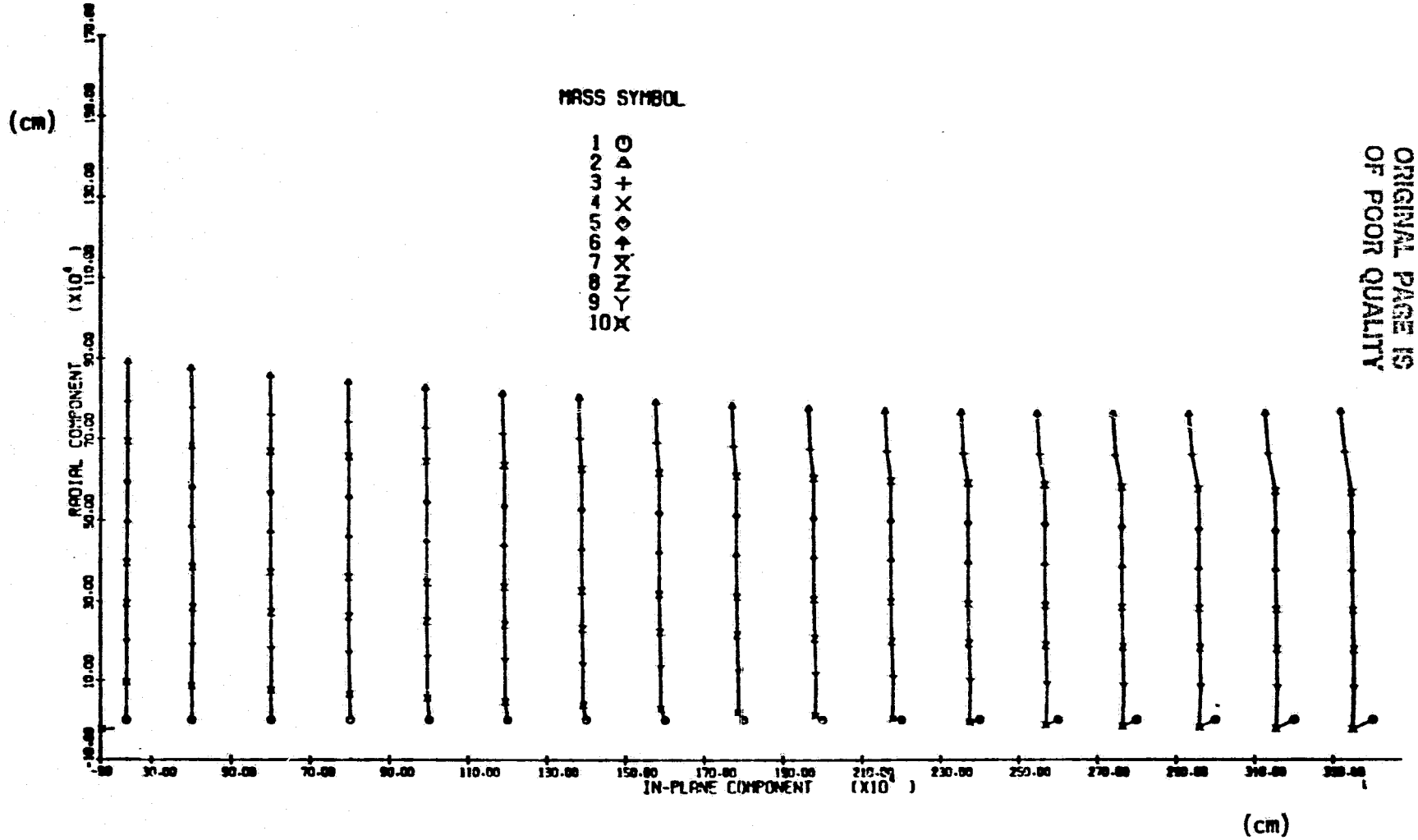

Figure 38. In-plane vs. radial behavior of the wire after a reel jam with 20 seconds between configurations. The deployment velocity was 10 m/sec and atmospheric drag is included.

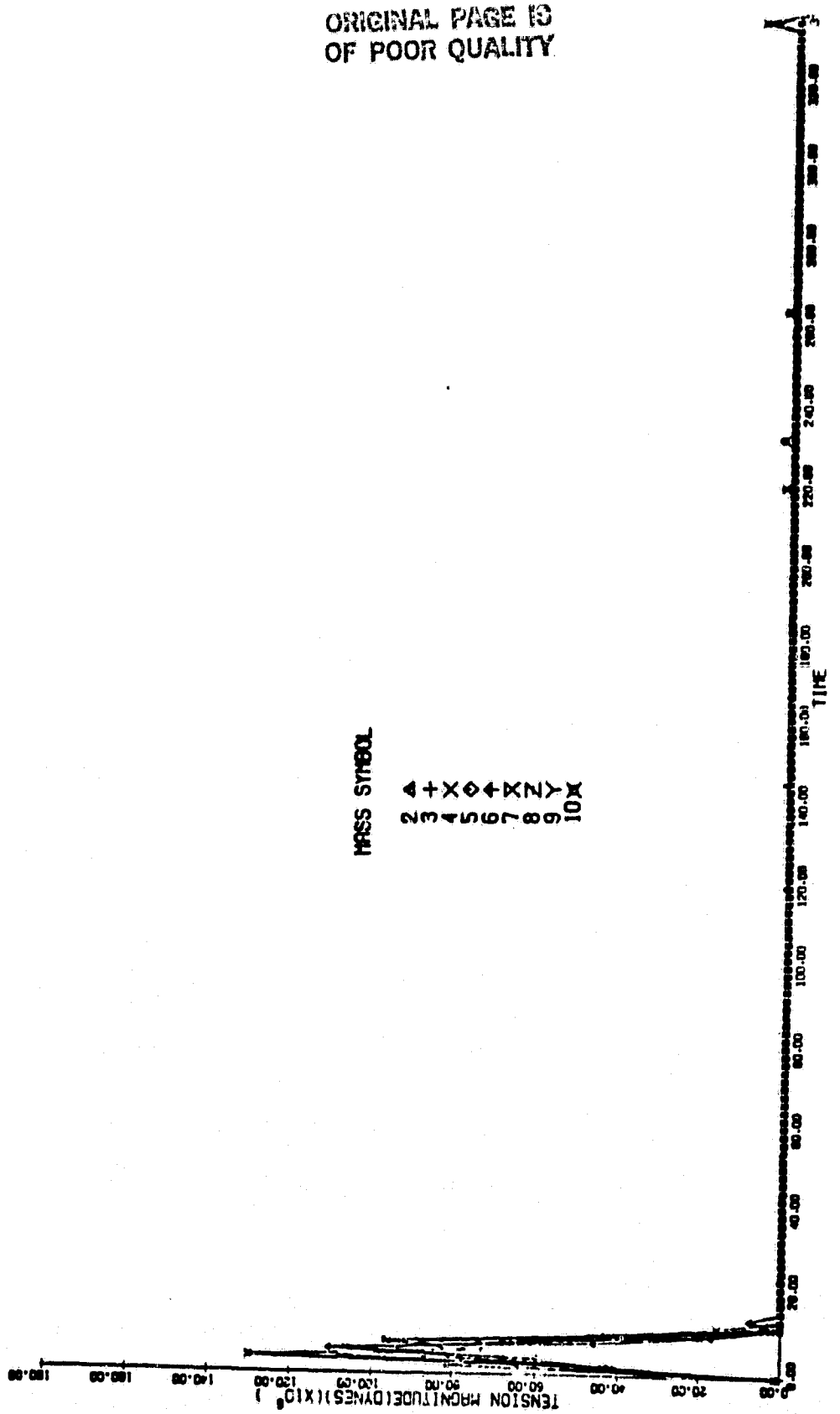

Figure 39. Tension vs. time at 2 second intervals after a reel jam. The deployment velocity was 10 m/sec and atmospheric drag is included.

tension as a function of time plotted at 2 second intervals. Several small tension spikes are evident during the time period. Many more tension spikes actually occurred between output points.

4.3 Tether Modelled as Eight Mass Points; Reel Jam at 90 km

In a long wire, the mass of the wire itself may be comparable to that of the payload at the end. In this case, the behavior of the wire after a reel jam may be qualitatively different. A run has been done with 10 mass points representing a 90 kilometer system being deployed at 20 m/sec. The tension vs. time for the first 50 seconds after a reel jam is shown in Figure 40. There is a significant spread in tension initially since the section of wire near the Shuttle (mass 10) must support the rest of the wire plus the payload. After the reel jam the tension wave travels up the wire to the subsatellite in about 17 seconds. The momentum of the subsatellite causes an increase of tension at about 18 seconds and this tension wave travels down the wire resulting in another tension increase at the Shuttle end at around 30 seconds. The system as a whole recoils to loss of tension after about 50 seconds. Figure 41 shows the radial position vs. time during the same time period. The initial value of each component has been subtracted from the subsequent values, and then the resultant curves separated from each other by 20 meters. The features described in Figure 40 can also be seen in this plot. The motion of the wire is arrested during the first 17 seconds. The momentum of the subsatellite causes an acceleration of the wire which travels down the wire arriving at the Shuttle end at about 30 seconds. The system then recoils to loss of tension after about 50 seconds.

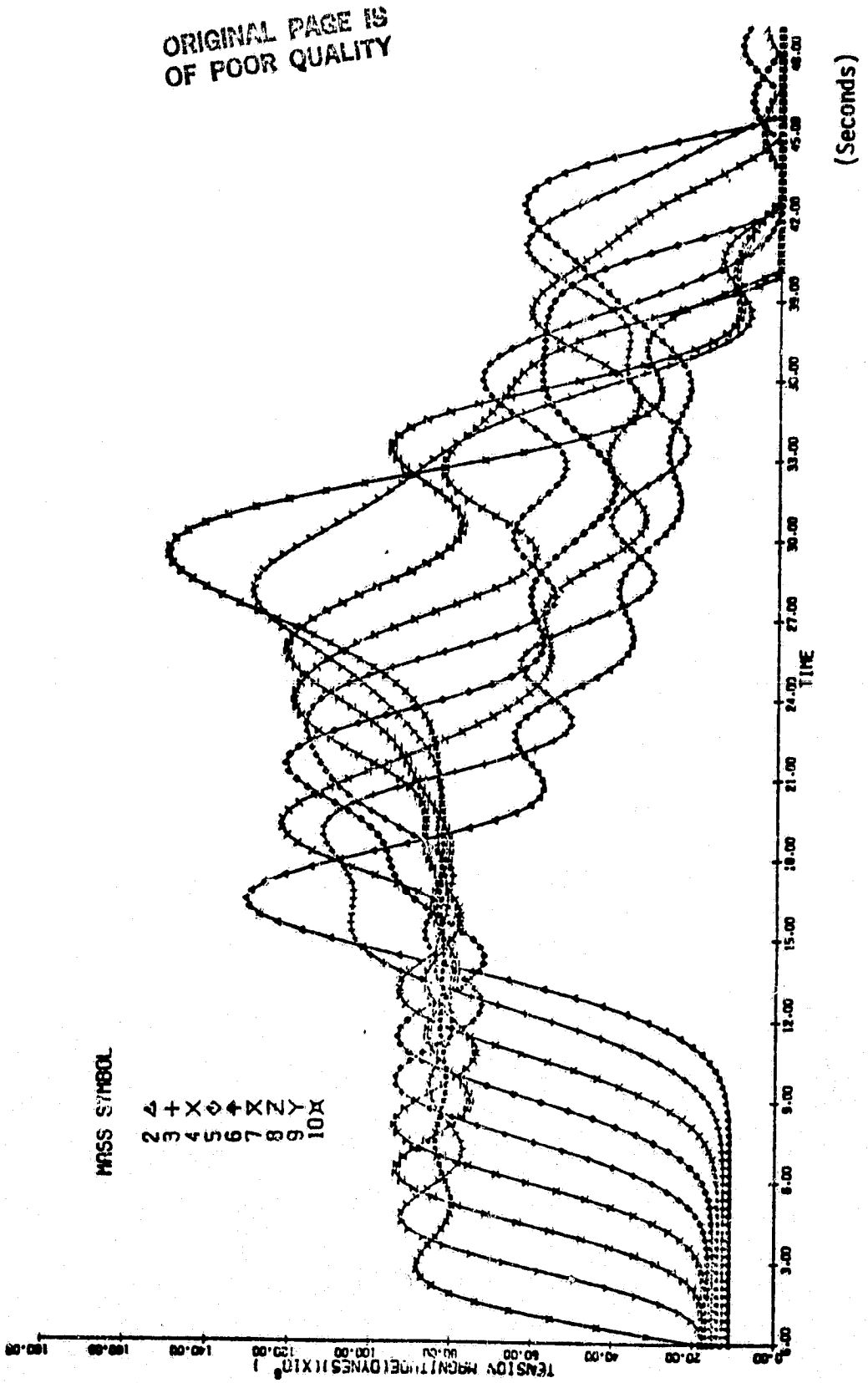

Figure 40. Tension vs. time after a reel jam in a 90 km wire during deployment at 20 m/sec.

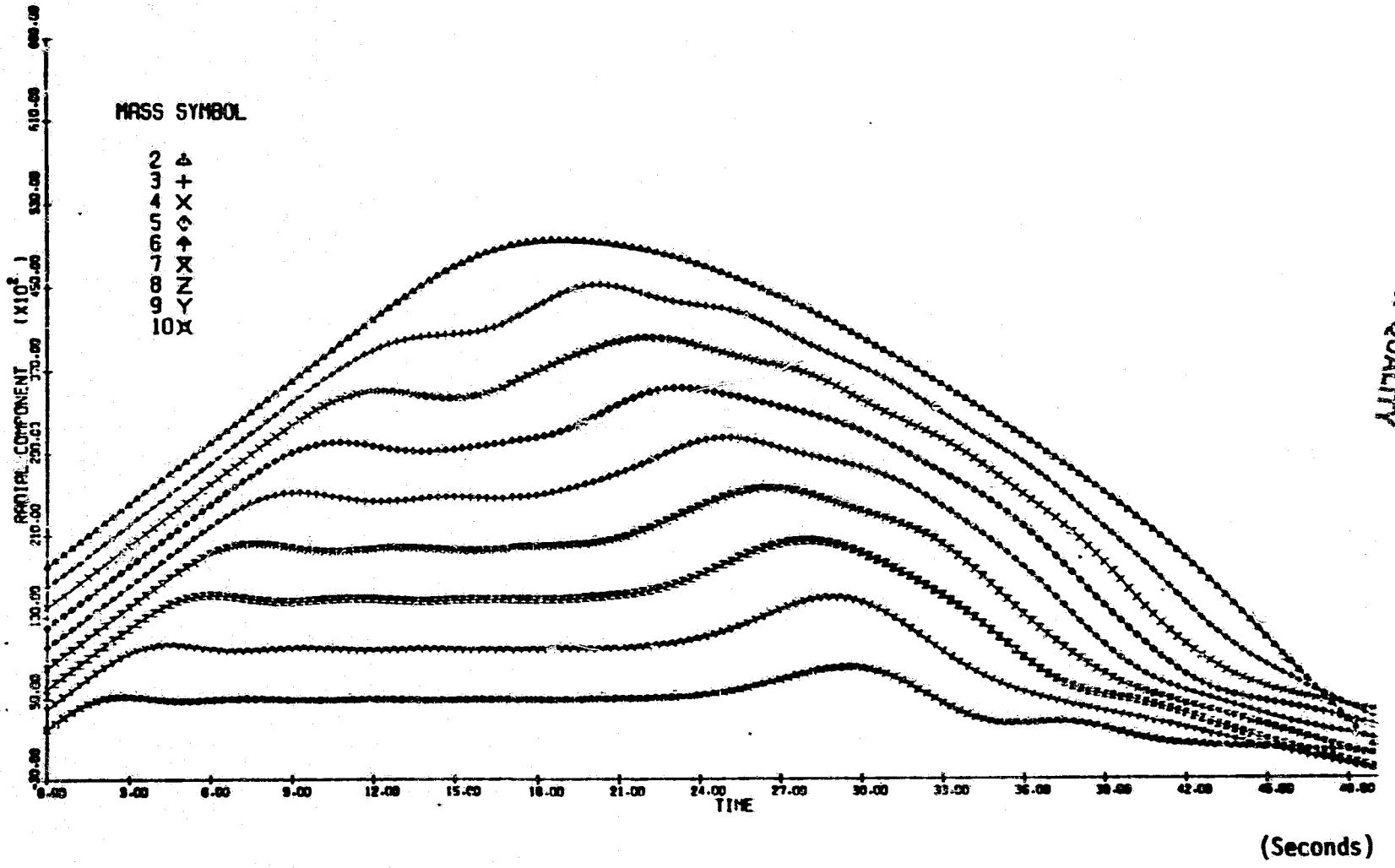

(cm)

Figure 41. Radial component vs. time after a reel jam in a 90 km wire during deployment at 20 m/sec. The initial value of each curve has been subtracted from the subsequent values and then each curve separated from the next by 20 meters.

5.0 Control of Rebound Behavior

5.1 Wire Break Case--Tapered Tether

One approach to the problem of recoil of a broken wire is to taper the tether so that it is thicker near the Shuttle end. This reduces the recoil in two ways. First, since the tether is thicker it is stiffer and stretches less under a given tension load. The stored energy E is $kx^2/2$. Since x is T/k, the energy is $T^2/2k$. Second, the mass of the tether increases with thickness so that the recoil velocity is reduced. Setting the kinetic energy equal to the energy stored in the stretch of the wire gives $mv^2/2 = T^2/2k$ or $v^2 = T^2/mk$. Since m and k are both proportional to the cross section A, we have $v \sim T/A$. It should be possible to protect the Shuttle from recoil in the event of a broken wire by proper design of the tether.

Further work in this area is needed. First, realistic values for damping and hysteresis in woven Kevlar tethers must be determined from the literature and by experimentation. Then methods for increasing the damping parameter should be investigated. Tapering of the tether can then be considered in light of all available alternatives.

5.2 Reel Jam Case--Subsatellite Damper

The simulations done to study the effect of a reel jam during deployment show the system rebounding and the wire going slack. Some simulations have been done to study the possibility of using a damper on the subsatellite to minimize recoil of the system. Such a damper would not affect the tension increases that result from the momentum of the wire, but could absorb the kinetic energy of the subsatellite. When the reel jams, a tension wave travels along the wire at the speed of sound. The tension is equal to the rate of change of momentum of the wire. If the elasticity is E, the density ρ, and cross section A, the deployment velocity is v_o, and the velocity of sound v_s is $\sqrt{E/\rho}$, then the rate of change of momentum along the wire is

$$T = \dot{p} = \dot{m}v_o = A\rho v_s v_o$$

$$= A\rho\sqrt{E/\rho}\, v_o = A\sqrt{\rho E}\, v_o$$

We have considered two methods of putting a damper on the subsatellite. One configuration consists of a spool of wire with a friction release that feeds wire out under constant tension whenever the stress in the tether exceeds the threshold. Such a system can be modelled in the SKYHOOK program by imposing a maximum value on the tension computed by the subroutine that models the elasticity of the wire. There is a slight complication in that the natural length of the wire segment will be increasing while the damper is reeling out wire. When the tension falls below the threshold, the new natural length must be determined at that point and used in subsequent calculations of the elastic tension force. A visco-elastic damper could be implemented in the form of a spring loaded reel of wire with viscous damping applied to the rotation of the reel. This configuration can be run directly in SKYHOOK because the modelling includes both damping and elasticity in calculating the tether tension.

Two runs have been done simulating a reel jam with a damper on the subsatellite. In the first case the motion is underdamped, and in the second case parameters for critical damping have been used. The initial conditions are obtained by starting with the equilibrium initial conditions for a reel jam with no damper and adding a short extra wire inserted by moving the subsatellite 20 meters further away from the Shuttle and putting another wire mass in its place. The 20 meter section was given parameters of $k = 1 \times 10^3$ and $b = 10^4$. For these values, the damping force is $bv = 10^4 \times 20 \times 10^2 = 20 \times 10^6$ dynes. The critical damping constant would be $2\sqrt{mk}$ which is 3.46×10^4 for a 300 kg satellite. Figure 42a shows the tension in the wire segments during the first 25 seconds after the reel jam, and Figure 42b is the tension during the period 25 - 50 seconds. Various sections of wire go slack during the first several seconds. The effect of the damper in reducing the amplitude of the oscillations between the masses can be seen especially in part a). The damper stretches from 20 meters to 265 meters during the first 25 seconds. As the subsatellite recoils to its original position the velocity is reduced to under 10 m/sec by the damping, but the wire would still go slack.

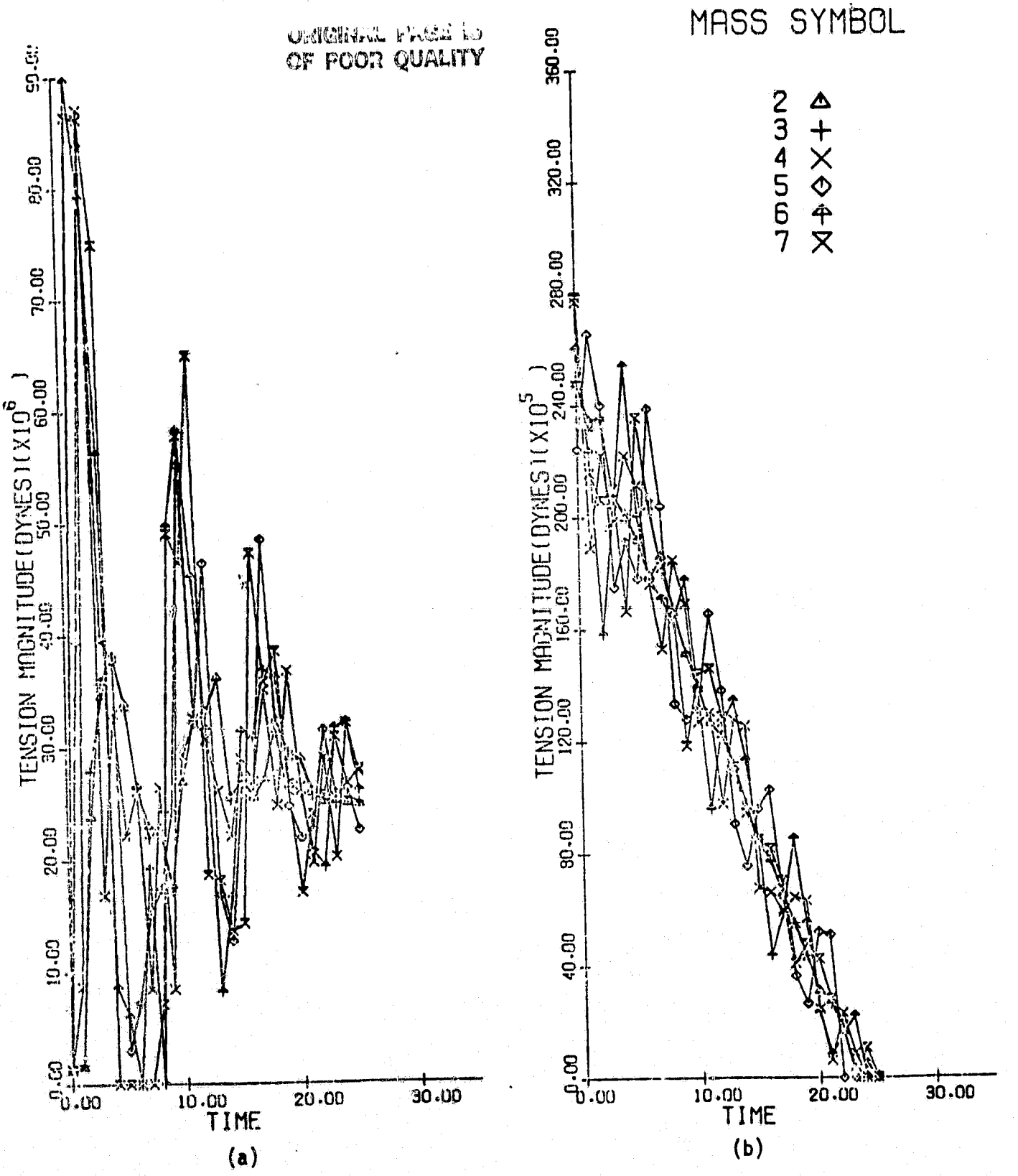

Figure 42. Tension vs. time after a reel jam with a damper on the subsatellite. The system is underdamped by about a factor of 3.5. Part a) is the period 0. - 25. seconds and part b) is 25. - 50. seconds.

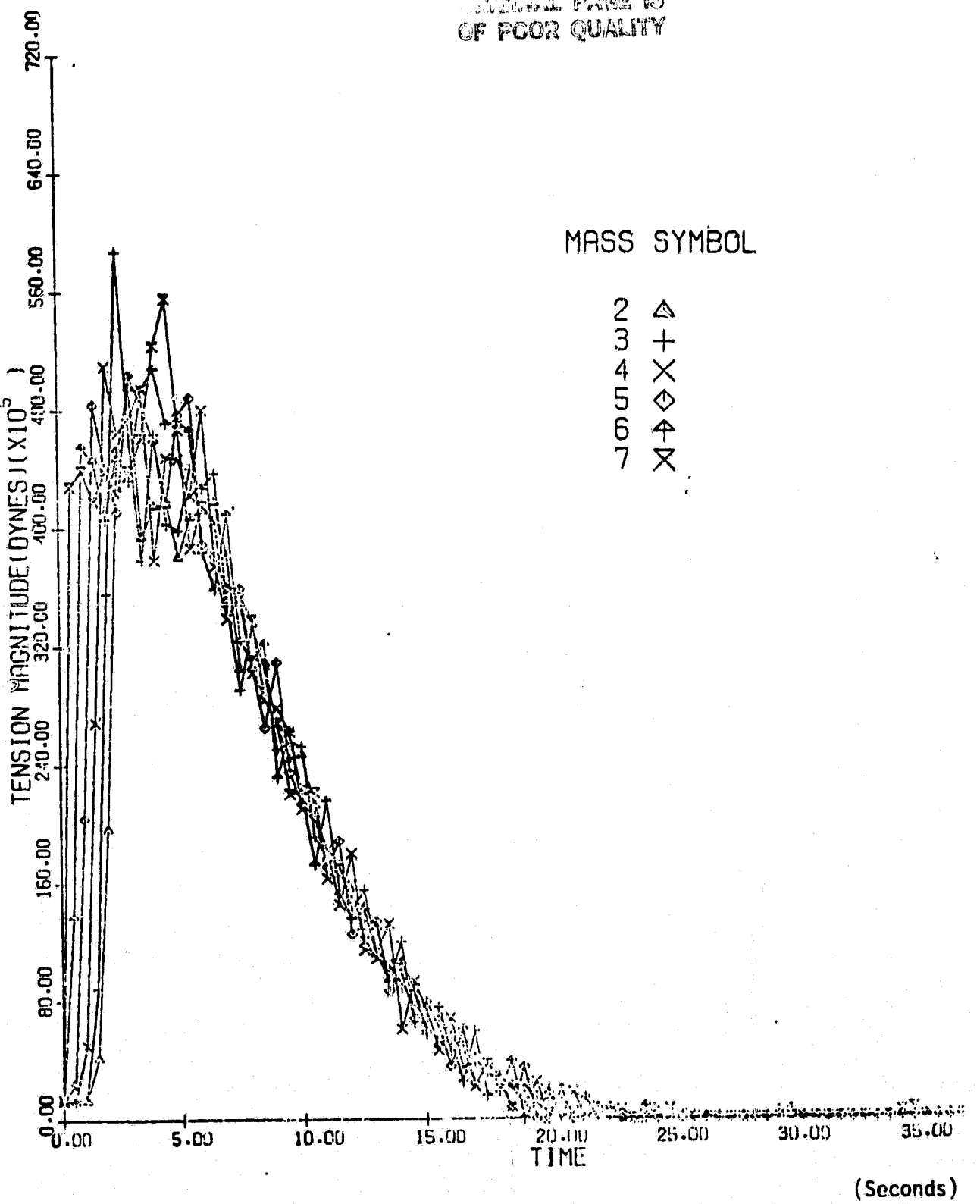

Figure 43. Tension vs. time after a reel jam with a damper on the subsatellite designed for critical damping.

A second run has been done with the parameters chosen for critical damping of a 300 kg mass. The condition for critical damping is that $b = 2\sqrt{mk}$. In order to avoid excessive tension from the damping, we can set a maximum T_M and chose $b = T_M/v_o$ where v_o is the deployment velocity. With $T_M = 50 \times 10^6$ dynes, we have $b = 5 \times 10^4$. The value of k required for critical damping is $k = b^2/4m$. For the particular values of the parameters, k = 2083 dynes/cm. The stiffness k is not an input parameter to the program, but can be controlled by selecting the values of E and A to satisfy the equation $k = EA/l_o$. The value of l_o is obtained by solving $T = k(l-l_o)$ for the natural length l_o and $A = 4.175 \times 10^{-6} cm^2$ with $E = .7 \times 10^{12}$. We are not concerned here with the actual physical implementation of the damper, and the value of A is only for convenience in the computer simulation. Figure 43 shows the tension as a function of time after a reel jam with critical damping. The damper stretches from 20 to 77 meters in the first 10 seconds. At 40 seconds the damper has returned to 28 meters and is recoiling at about 1.4 m/sec. The mass next to the damper is recoiling at about .4 meters/sec and there is about 8 meters of slack in the wire. This behavior is much more stable than the behavior without a damper although still not perfect.

The damper is in series with the wire which is assumed perfectly elastic. If the wire is stretched by the end mass, this energy will go into recoil of the system. One technique for minimizing recoil is to reduce both the stiffness and damping coefficient so that the damper stretches more under lower tension. The limiting factor in this approach is the amount of line stored in the spool on the subsatellite.

The radial vs. in-plane behavior for the underdamped case is shown in Figure 44. Deployment of additional tether by the damper is clearly shown in this Figure which has an expanded horizontal scale to exaggerate the motion of the tether. Actual in-plane motion is about 10 meters at 25 seconds in this Figure for an angular displacement of 1×10^{-3} radians as seen from the Shuttle. The damper controls the recoil completely by deploying 256 meters of additional tether in 23 seconds. It reduces maximum tension by a factor of four with respect to the undamped case.

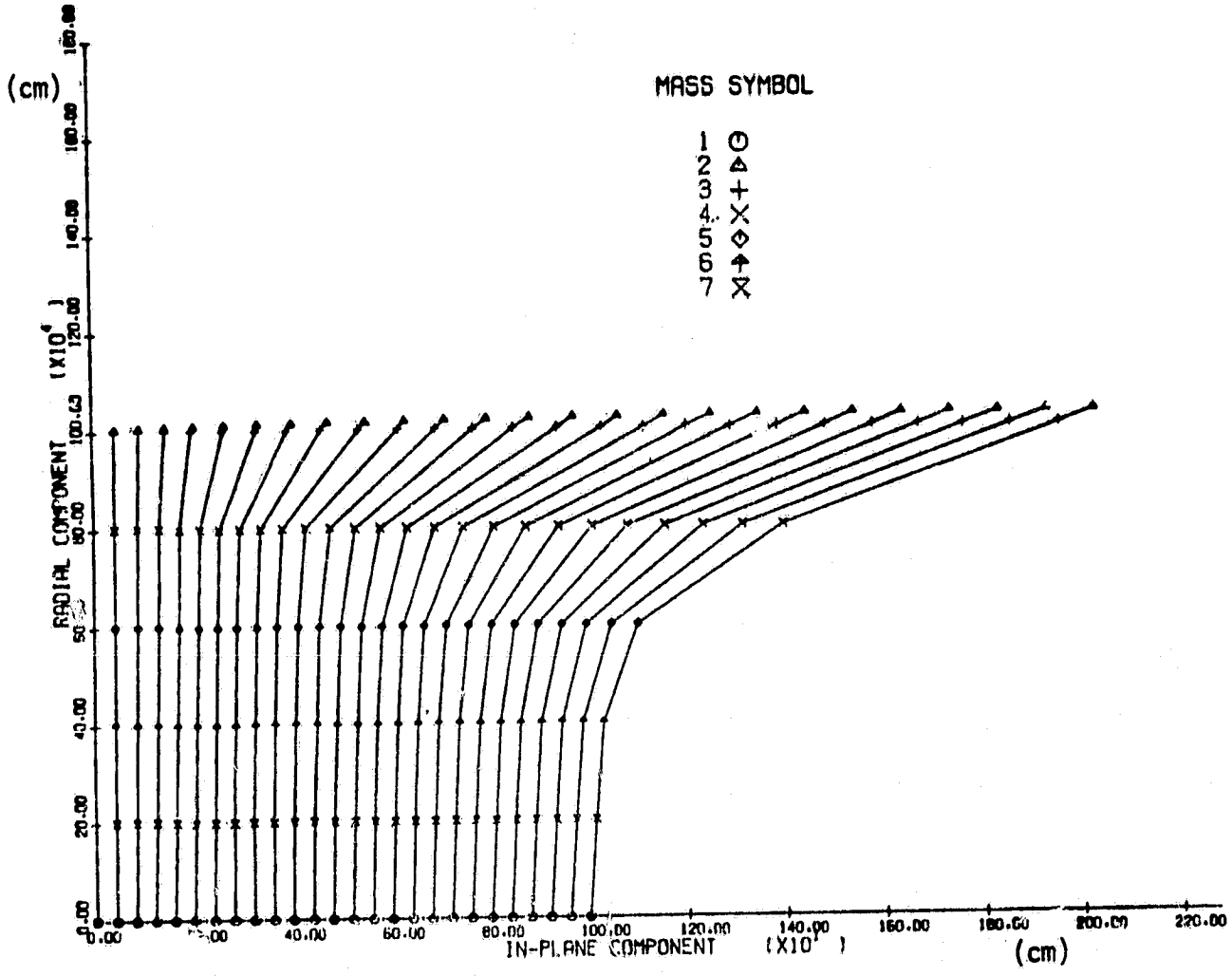

Figure 44. Control of tether recoil by means of a damper on the subsatellite.